CCL3 promotes germinal center B cells sampling by follicular regulatory T cells and ensures optimal humoral response.

Zachary L. Benet[1], Fang Ke[1], Matangi Marthi[1], Rita Wu[1], Jackson S. Turner[1], Jahan B. Gabayre[1], Michael I. Ivanitskiy[1], Sahil S. Sethi[1], and Irina L. Grigorova[1*].

[1]Department of Microbiology and Immunology, University of Michigan Medical School, 1150 West Medical Center Drive, 5641 Medical Science II, Ann Arbor , Michigan 48109-5620

[*]Please address correspondence to:
Irina L. Grigorova
1150 W. Medical Center Dr
6748 MSII
Ann Arbor, MI 48109
(734) 615-3882 (p)
(734) 764-3562 (f)
igrigor@umich.edu
ORCID: 0000-0002-4963-7403

ABSTRACT

A hallmark of adaptive humoral immunity is formation of germinal centers (GC), the site of B cell antigen-dependent clonal expansion, immunoglobulin diversification, and affinity maturation. This set of coordinated processes is dependent on follicular T cells and leads to generation of memory cells and long-lived plasma cells that secrete high-affinity antibodies (Abs). Despite the wealth of studies dissecting the chemotactic cues that organize GCs, it is unclear whether GC B cells may secrete additional factors that enable their efficient sampling by follicular T cells. In this work we show that in mice a small subset of GC centrocytes upregulates expression of proinflammatory chemokines CCL3/4. We also demonstrate that GC B cells-intrinsic production of CCL3 promotes their direct interactions with follicular regulatory T cells (Tfr), but not follicular helper T cells (Tfh) *in vivo*. Finally, we show that GC B cells-intrinsic production of CCL3 is required for optimal control of GC and plasma cell responses.

INTRODUCTION

CCL3 and CCL4 (MIP1-α and MIP1-β) are proinflammatory chemokines that are secreted by various types of immune cells upon activation and play important roles in inflammatory responses and multiple other processes (Menten, Wuyts et al. 2002, Maurer and von Stebut 2004). In B cell cultures with naive, memory, or GC B cells, the cross-linking of B cell receptors (BCRs) upregulates expression and secretion of CCL3/4 (Krzysiek, Lefevre et al. 1999, Bystry, Aluvihare et al. 2001). In addition, analysis of published GC microarray data suggests that expression of CCL3/4 may be elevated in GC centrocytes compared to centroblasts (Caron, Le Gallou et al. 2009, Compagno, Lim et al. 2009, Victora, Dominguez-Sola et al. 2012). Despite multiple indications that CCL3/4 is secreted by activated and GC B cells, the significance of B-cell intrinsic production of proinflammatory chemokines for regulation of humoral response is unclear.

In 2001 Bystry et al. demonstrated that a subset of splenic CD4 T cells that were CD25^{high}, expressed high levels of TGF-β and CTLA-4, and had a suppressive phenotype *ex vivo,* could migrate to CCL4 (but not CCL3) in transwell assays. The above observations raised the possibility that CCL4 may promote Tregs' interactions with activated B cells or dendritic cells (which also produce CCL3/4) to regulate B cell responses. However, whether more recently identified subset of follicular resident Tregs

67 can respond to CCL3 or CCL4 has been unclear (Lim, Hillsamer et al. 2005, Alexander,
68 Tygrett et al. 2011, Chung, Tanaka et al. 2011, Linterman, Pierson et al. 2011).
69
70 Tfr cells are a subset of FoxP3^{pos} Tregs that play a role in the control of GC responses.
71 While the majority of Tfr cells arise from natural Tregs, some can be induced from
72 foreign antigen-specific Th cells (Aloulou, Carr et al. 2016). Similarly to Tfh cells, Tfr cells
73 develop in the secondary lymphoid organs following foreign antigen challenge, express
74 the transcription factor Bcl6, upregulate surface expression of CXCR5, PD1 and ICOS
75 receptors, and localize to the follicles and the GCs (Chung, Tanaka et al. 2011,
76 Linterman, Pierson et al. 2011, Wollenberg, Agua-Doce et al. 2011). Tfr cells appear to
77 play a dual role in the control of GC responses. Deficiency in Tfr cells has been reported
78 to induce a 1.5 to 2-fold increase in GC size at the peak of GC response (Chung,
79 Tanaka et al. 2011, Linterman, Pierson et al. 2011, Wollenberg, Agua-Doce et al. 2011),
80 to affect Tfh cell's cytokine production and Ab class-switching (Sage, Francisco et al.
81 2013, Sage, Paterson et al. 2014, Wu, Chen et al. 2016), to increase recruitment of non-
82 foreign Ag-specific B cell clones into GCs (Linterman, Pierson et al. 2011, Wu, Chen et
83 al. 2016), and to promote development of self-reactive antibodies (Wu, Chen et al. 2016,
84 Botta, Fuller et al. 2017) and even autoimmunity in influenza-infected mice (Fu, Liu et al.
85 2018). At the same time, Tfr cells have been shown to improve affinity maturation and
86 secondary Ab responses in mice (Linterman, Pierson et al. 2011, Wu, Chen et al. 2016).
87 Moreover, Tfr cells-produced IL10 has been recently demonstrated to elevate expression
88 of FOXO1 in GC B cells, promote formation of dark zone GC centroblasts and thus to
89 sustain GC responses (Laidlaw, Lu et al. 2017). While multiple mechanisms of Tfr cells'
90 action have been suggested based on the *in vivo* and *ex vivo* studies (Alexander, Tygrett
91 et al. 2011, Sage, Francisco et al. 2013, Sage, Paterson et al. 2014, Wing, Ise et al.
92 2014, Wing and Sakaguchi 2014, Sage, Ron-Harel et al. 2016), whether *in vivo* Tfr cells
93 only regulate Tfh cells and thus indirectly control GC responses or can also act on the
94 GC B cells directly remains an open-ended question.
95
96 Here we investigated the role of B cell-intrinsic production of CCL3 in the regulation of
97 GC responses. Based on 2-photon imaging of murine lymph nodes we found that
98 production of CCL3 by GC B cells promotes their sampling by Tfr cells. Consistent with
99 CCL3's role in mediating GC-Tfr cells interactions, we found that immunized CCL3-

100 deficient mice develop a small increase in GC responses compared to WT mice and
101 have reduced secondary Ab responses. Our data also suggests that CCL3 deficiency in
102 foreign antigen-specific GC B cells leads to their decreased selection in GCs and
103 development of plasma cells. Based on these findings we suggest that CCL3 production
104 by GC B cells is required for optimal foreign antigen-specific GC B cell responses.
105
106 **RESULTS**
107 **A small subset of GC centrocytes upregulates expression of CCL3 and CCL4.**
108 Based on the previous microarray data (Caron, Le Gallou et al. 2009, Compagno, Lim et
109 al. 2009, Victora, Dominguez-Sola et al. 2012) GC centrocytes (CC) may have elevated
110 expression of CCL3/4 compared to centroblasts (CB). To verify expression of *Ccl3* and
111 *Ccl4* in murine GC B cells, we performed qRT-PCR analysis of GC CC, CB and non-GC
112 B cells sorted from the draining lymph nodes (dLNs) of immunized mice at 10 days post
113 immunization (d.p.i) (**Fig. 1a**). Consistent with previous microarray analysis, we found
114 that expression of CCL3/4 is upregulated in murine GC CC compared to CB (**Fig. 1b, c**).
115 To determine whether CC have uniform expression of CCL3/4 or only a few CCs
116 upregulate CCL3/4 production *in vivo*, we performed single cell qPCR analysis of GC
117 CC, CB and non-GC B cells at 10 d.p.i. We found that the majority of CC and CB had
118 comparable expression of CCL3 and CCL4 (**Fig. 1d, e**). However, a small fraction of GC
119 CC (12% in experiment 1 and 9% in experiment 2) had upregulated expression of
120 CCL3/4 (**Fig. 1d-i**). The increased CCL3/4 expression in a subset of cells was observed
121 regardless of whether B2m or HPRT1 housekeeping genes were used for normalization
122 (**Fig. 1f-i**). In addition, while CCL3/4 expression in CB and naïve B cells were best
123 described by a single Gaussian distribution (**Fig. 1j, k**), based on the maximal likelihood
124 analysis two or more Gaussian distributions were required to fit GC CC data (**Fig. 1l,** in
125 Experiments I and II). The data suggests that increased expression of CCL3/4 detected
126 in bulk GC CC vs. CB occurs due to a small subset of GC CC that have upregulated
127 expression of CCL3/4 *in vivo*.
128
129 **Increased GC response in CCL3-KO mice.**
130 To determine if CCL3 plays a role in the regulation of GCs, we utilized CCL3-KO mice
131 (Cook, Beck et al. 1995). In unimmunized CCL3-KO and WT mice we observed no

132 significant difference in the GC B cells numbers in peripheral lymph nodes (pLNs),
133 spleens, mesenteric LNs (mLNs) and peyer patches (PP) (**Fig. 2a**). However, at 10 d.p.i.
134 we detected a small, but significant increase in the GC response in the dLNs of CCL3-
135 KO mice compared to WT that was independent of the antigen or the adjuvant used
136 (**Fig. 2b-e**). We then tested whether in littermate-control CCL3$^{-/-}$ mice GCs were also
137 elevated compared to CCL3$^{+/+}$, and confirmed the observed phenotype (**Fig. 2f, g)**.
138 Interestingly, treatment of WT or CCL3-KO mice with CCL4-neutralizing antibodies
139 during formation of GCs, at 7 d.p.i., did not lead to further increase in the GC response
140 (**Supplementary Fig. 2**). The observed accumulation of GC B cells at 10 d.p.i. was not
141 due to significant changes in formation of Tfh and Tfr cells or in their ratio (**Fig. 2h-j**). In
142 addition, the increase in GC B cells did not lead to significant rise in the numbers of
143 plasmablasts (PB) at 10 d.p.i. (**Fig. 2k, l**).
144
145 **Foreign antigen-specific Ab response in CCL3-KO mice.**
146 To study foreign antigen-specific Ab response we immunized CCL3$^{+/+}$ and CCL3$^{-/-}$
147 littermate control mice with NP-KLH in Ribi adjuvant and boosted them at 24 d.p.i. At 15
148 and 21 d.p.i. we detected no significant difference in NP-specific IgG1 Abs (**Fig. 3a, b**).
149 However, at 4 days following the boost with NP-KLH in Ribi, the overall titers of NP-
150 specific IgG1 Abs in CCL3$^{+/+}$ mice were significantly higher than in CCL3$^{-/-}$ littermate
151 controls (**Fig. 3a**, **day 28**). Interestingly, the fraction of higher-affinity (NP2-binding) Abs
152 in CCL3$^{-/-}$ mice was increased (**Fig. 3b, c, day 28**). In addition, while no significant
153 difference in the total IgG1, IgG2b and IgG2c Abs was detected at 28 d.p.i. (**Fig. 3d-f**),
154 we found an increase in the fraction of total, but not NP-specific, IgA Abs in CCL3$^{-/-}$ mice
155 (**Fig. 3g, h**).
156
157 **CCL3 and CCL4 induce chemotaxis of follicular regulatory T cells *ex vivo.***
158 To determine whether CCL3 may promote chemotaxis of Tfh and/or Tfr cells *ex vivo* we
159 performed transwell migration analysis of CD4 T cells isolated from dLNs of mice at 10
160 d.p.i. with OVA in Ribi adjuvant. CXCR5^{high} PD1^{high} FoxP3^{+} Tfr cells transmigrated in
161 response to CCL3 chemokine (**Fig. 4a, b**). Similar trends were observed for CXCR5^{low}
162 PD1^{low} FoxP3^{+} and CXCR5^{int} PD1^{int} FoxP3^{+} CD4 T cells (**Fig. 4a, b**). We also observed
163 transmigration of Tfr and other regulatory T cell subsets to CCL4 (**Fig. 4c**). The observed
164 transmigration was predominantly due to chemotaxis rather than chemokinesis, since

165 addition of CCL3 or CCL4 chemokines to both the upper and the lower wells of the
166 transwell chamber did not promote Tregs' transmigration (**Fig. 4b, c**). No significant
167 transmigration of Tfh cells (CXCR5^{high} PD1^{high} FoxP3^{-}) to CCL3 and CCL4 chemokines
168 was observed (**Fig. 4d, e**). These data suggest that CCL3 and CCL4 can induce
169 chemotaxis of Tfr and possibly other Treg cells *ex vivo*.
170
171 **Adoptively transferred Tregs can become Tfrs' and be visualized by 2P**
172 **microscopy.** We then asked whether CCL3 could promote individual interactions of Tfr
173 cells with GC B cells *in vivo*. To directly test this, we developed an imaging strategy that
174 enabled visualization of adoptively transferred Tregs within the GC-containing follicles of
175 living mice using 2-photon (2P) microscopy (**Fig. 5a**). Because intravenous injection of
176 Tregs is insufficient to get enough of the transferred Tregs into peripheral LNs for
177 microscopy analysis, we utilized the fact that adoptively transferred Tregs undergo
178 proliferation in recipient FoxP3^{DTR} mice upon diphtheria toxin (DTx)-induced ablation of
179 DTx receptor (DTR)-expressing resident Tregs (Kim, Rasmussen et al. 2007). Of note,
180 while treatment of FoxP3^{DTR} mice with DTx leads to development of severe autoimmune
181 disease, pre-transfer of 10^6 polyclonal Tregs rescues FoxP3^{DTR} mice from autoimmunity
182 (Kim, Rasmussen et al. 2007). To generate mice with a high number of brightly
183 fluorescent Tfr cells, we first transferred 10^6 polyclonal Tregs that expressed both Foxp3-
184 GFP and tdTomato into Foxp3^{DTR} mice (Bettelli, Carrier et al. 2006, Kim, Rasmussen et
185 al. 2007). We then treated the Foxp3^{DTR} recipients with 5 μg of DTx two times, one week
186 apart. As reported before, following transient ablation of Foxp3^{DTR} Tregs, the adoptively
187 transferred Tregs as well as the remaining endogenous Tregs underwent vigorous
188 proliferation. At 14 days following the initial DTx treatment, tdTomato Tregs represented
189 about 50% of all Tregs in the blood (**Fig. 5b**). We then co-transferred Duck Egg
190 Lysozyme (DEL)-specific HyHEL10 B cells expressing CFP, OVA-specific OTII CD4 T
191 cells expressing GFP, as well as non fluorescent HyHEL10 B and OTII T cells into the
192 same recipient mice and induced their recruitment into the GCs by s.c. immunization
193 with DEL-OVA as previously described (Allen, Okada et al. 2007). By 8 d.p.i. the overall
194 levels of Tregs in the blood had returned to normal (**Fig. 5b**). Based on confocal and flow
195 cytometry analysis we determined that over a fifth of CD4^{+}Foxp3^{+} cells from dLNs
196 expressed tdTomato and that tdTomato^{+} cells were almost exclusively Foxp3^{+} (**Fig. 5c,**
197 **d**). Additionally, tdTomato^{+} Foxp3^{+} cells that were also CXCR5^{high} PD1^{high} had increased

198 expression of Bcl6^{+} as expected for Tfr cells (**Fig. 5c**). At 7-8 d.p.i. a relatively minor
199 fraction of GC-proximal Tfr cells entered into the GCs, while majority of the cells moved
200 around GCs in proximity to the outer edge GC B cells (**Fig. 5e, Supplementary Movie**
201 **1**). These data suggest that the adoptive transfer of fluorescent Tregs followed by
202 transient ablation of non-fluorescent endogenous Tregs and immunization is sufficient to
203 visualize Tfr cells within GC-associated follicles in living mice by 2P microscopy.
204
205 **GC B cells' CCL3 promotes their contacts with Tfr, but not Tfh cells *in vivo*.**
206 To determine whether GC B cells' intrinsic production of CCL3 promotes their direct
207 interactions with Tfr cells or with Tfh cells *in vivo* we utilized the experimental setup
208 developed by us (**Fig. 5**) and in previous work (Allen, Okada et al. 2007) and outlined in
209 **Figures 6a** and **b**. For analysis of T cell interactions with CCL3$^{+/+}$ and CCL3$^{-/-}$ GC B
210 cells, recipient mice were co-transferred with CCL3$^{+/+}$ HyHEL10 B cells that expressed
211 CFP and CCL3$^{-/-}$ HyHEL10 B cells that expressed GFP. To determine Tfr cells'
212 interactions with GC B cells we tracked tdTomato^{+} Tfr cells when they contacted or
213 passed through the GCs, and analyzed their interactions with fluorescent CCL3$^{+/+}$ and
214 CCL3$^{-/-}$ foreign Ag-specific HyHEL10 B cells within the same GCs (**Fig. 6c,**
215 **Supplementary Movie 2**). To take into account the ambiguity of correct identification of
216 B-T cell interactions by 2P imaging, we used both "strict" and "non-strict" definitions of
217 contacts between GC B cells and follicular T cells. By "strict" we define the interactions
218 that based on the cell colocalization analysis in 3D have taken place with high
219 confidence. By "non-strict" interactions we identify all likely interactions identified based
220 on cell proximity, including the "strict" interactions. The data was analyzed in a blinded
221 fashion to avoid possible bias in cell contact definition (**Fig. 6d, Supplementary Movie**
222 **3**). We calculated the normalized contact frequency (NCF) of Tfr cells with fluorescent
223 CCL3$^{+/+}$ and CCL3$^{-/-}$ GC B cells by dividing the total number of Tfr cell contacts with
224 CCL3$^{+/+}$ or CCL3$^{-/-}$ GC B cells by the average numbers of fluorescent B cells of each type
225 present in the imaged GCs. Tfr cells' NCF was lower for CCL3$^{-/-}$ compared to CCL3$^{+/+}$
226 GC B cells in 5 experiments, independently of the "strict" vs "non-strict" B-Tfr cell contact
227 definition (**Fig. 6e-h**). The differences in Tfr cell contact frequencies with CCL3$^{+/+}$ and
228 CCL3$^{-/-}$ GC B cells were not due to distinct migratory properties of CCL3$^{+/+}$ and CCL3$^{-/-}$ B
229 cells (**Supplementary Fig. 6**). In contrast to Tfr cells, OTII Tfh cell NCF with CCL3$^{+/+}$ vs.

230 CCL3$^{-/-}$ GC B was comparable (**Fig. 6e-h, Supplementary Movie 4**). The ratio of T
231 cells' NCF with CCL3$^{+/+}$ vs. CCL3$^{-/-}$ GC B cells was significantly lower for Tfh compared
232 to Tfr cells (**Fig. 6f, h)**.
233
234 While Tfr cells formed more frequent contacts with CCL3$^{+/+}$ GC B cells, duration of Tfr
235 cell interactions with CCL3$^{+/+}$ and CCL3$^{-/-}$ GC B cells was comparable (**Fig. 6i, j**).
236 Additionally, no significant difference in the duration of Tfh cell contacts with CCL3$^{+/+}$ vs.
237 CCL3$^{-/-}$ GC B cells was observed (**Fig. 6i, j**). The vast majority of Tfr and Tfh cell
238 contacts with GC B cells were shorter than 5 min (**Fig. 6i-l**). However, while a substantial
239 number of both Tfh and Tfr cells also formed more prolonged interactions with GC B
240 cells, no Tfr cells' interactions with GC B cells exceeding 7.5 min were observed (**Fig.
241 6k, l, Supplementary Movies 3, 4**).
242
243 **Transient depletion of Tregs leads to relative increase in CCL3$^{+/+}$ vs. CCL3$^{-/-}$**
244 **HyHEL10 GC B cells at the peak of GC response.** To determine whether Tfr cells may
245 act on CCL3-proficient GC B cells and modulate their participation in GC response we
246 sought to determine whether transient depletion of Tregs after formation of GCs could
247 affect relative involvement of CCL3 proficient and deficient B cells in the GC response. In
248 order to test that, we co-transferred CCL3$^{+/+}$ and CCL3$^{-/-}$ HyHEL10 B cells into recipient
249 FoxP3^{DTR} mice, immunized mice to promote HyHEL10 cell entry into GC response and
250 then treated mice with diphtheria toxin (DTx) to promote transient depletion of FoxP3^{+}
251 cells or with PBS for control (**Fig. 7a**). We hypothesized that CCL3 secreted by GC B
252 cells promotes their direct interactions with and inhibition by Tfr cells. In that case,
253 depletion of Tfr cells should lead to increased expansion of CCL3-proficient compared to
254 CCL3-deficient GC B cells (**Fig. 7b**). As expected, treatment of the recipient mice with
255 DTx at 6 d.p.i. led to significant drop in Tfr cells numbers in 3 days (**Fig. 7c, d**) and small
256 increase in the GC B cell numbers (**Fig. 7e**). Consistent with that, upon the transient Tfr
257 cell depletion, we detected a small increase in CCL3$^{+/+}$ HyHEL10 B cell numbers,
258 however CCL3$^{-/-}$ HyHEL10 GC B cells were virtually unchanged (**Fig. 7f**). As a result of
259 this, there was significant enrichment of CCL3$^{+/+}$ vs. CCL3$^{-/-}$ HyHEL10 B cells within GCs
260 (**Fig. 7g**). Therefore, the data is consistent with direct CCL3-dependent inhibition of GC
261 B cells by Tregs at the peak of GC response (**Fig. 7b**).
262

263 **CCL3$^{+/+}$ foreign-Ag specific B cells outcompete CCL3$^{-/-}$ B cells in GCs and PB**
264 **response overtime.** Previous study suggested that Tfr cells plays a dual role in GC
265 responses and may promote positive selection of B cells within GCs (Laidlaw, Lu et al.
266 2017). We therefore examined participation of CCL3$^{+/+}$ and CCL3$^{-/-}$ HyHEL10 B cells in
267 the GC and PB response overtime (**Fig. 8a**). At 6 d.p.i. about 2 times more CCL3$^{+/+}$
268 compared to CCL3$^{-/-}$ HyHEL10 B cells entered into the GC response (**Fig. 8b**, the gating
269 strategy is outlined in **Supplementary Fig. 8a**). Interestingly, at that time we observed a
270 trend for increased formation of PB relative to GC B cells by CCL3-deficient HyHEL10 B
271 cells (**Fig. 8c**, **Supplementary Fig. 8b, c; day 6**). By 8 d.p.i. CCL3$^{+/+}$ and CCL3$^{-/-}$
272 HyHEL10 cell participation in GCs and formation of PB was comparable (**Fig. 8b, c; day**
273 **8**). However, starting at 12 d.p.i. CCL3$^{-/-}$ HyHEL10 cells dropped out of the GC and PB
274 response more rapidly than CCL3$^{+/+}$ HyHEL10 cells (**Fig. 8b, c; days 12, 15**).
275 Preferential selection of CCL3$^{+/+}$ vs. CCL3$^{-/-}$ HyHEL10 GC B cells was observed
276 independently of the cyan fluorescent protein (CFP) or green fluorescent protein (GFP)
277 expression by HyHEL10 cells (**Supplementary Fig. 8d**). In accord with previously
278 proposed role for Tfr cells in contributing to the selection of GC B cells, depletion of Tfr
279 cells at 12 d.p.i. led to decreased selection of CCL3$^{+/+}$ relative to CCL3$^{-/-}$ HyHEL10 B
280 cells at 15 d.p.i. (**Fig. 8d-f**). Overall, these findings suggest that Tfr may act on foreign
281 Ag-specific GC B cells in CCL3 chemokine-dependent fashion and promote both modest
282 inhibition of their expansion at the peak of GC response, as well as their selection at the
283 later time points.
284
285 **DISCUSSION:**
286 Multiple chemotactic signals produced by follicular dendritic cells and other stromal cells,
287 have been shown to orchestrate GC's anatomy and contribute to optimal cell migration
288 between GC zones and to cell retention within GCs (Allen, Okada et al. 2007, Pereira,
289 Kelly et al. 2009, Green, Suzuki et al. 2011). However, whether GC B cells themselves
290 may produce chemotactic signals that direct their interactions and control by follicular T
291 cells, has not been addressed. In this study we found that a subset of GC CC upregulate
292 expression of proinflammatory chemokines CCL3/4. We also show that Tfr cells respond
293 to CCL3/4 chemokines *ex vivo* and form more frequent contacts with CCL3-proficient vs.
294 CCL3-deficient GC B cells *in vivo.* Our studies also suggest that CCL3 production by

295 foreign Ag-specific GC B cells is important for their negative control by Tfr cells as well
296 as for their prolonged participation in the GC and PB response.
297
298 We suggest two possible models that could explain the increased sampling of CCL3-
299 proficient GC B cells by Tfr cells (**Fig. 9**). First, the observed effect could be due to local
300 chemoattraction of Tfr cells to a subset of CCL3-secreting B cells within GCs. Since BCR
301 crosslinking has been reported to induce upregulation of CCL3/4 production in GC B
302 cells (Krzysiek, Lefevre et al. 1999), we hypothesize that GC centrocytes that recently
303 acquired antigen from FDCs (and possibly T cell help) are likely to produce more CCL3/4
304 than other GC B cells, and thus could form local short-range gradients of these
305 chemokines (**Fig. 9a**). In that case, to preserve local CCL3 gradient around migrating
306 GC B cell, secreted CCL3 would have to be rapidly internalized and removed by other
307 cells within GCs. Alternatively to the first model, CCL3 chemokine secreted by GC B
308 cells could be transiently immobilized on the surface of selected GC B cells in
309 association with chemokine-binding glycosaminoglycans (Liang, Triandafillou et al. 2016)
310 and may serve to stabilize very transient probing interactions of GC B cells with Tfr cells
311 that are beyond the resolution capabilities of intravital 2P microscopy (**Fig. 9b**). Both of
312 these models can lead to decreased efficiency in productive sampling of CCL3 KO B
313 cells by Tfr cells. Since our intravital imaging system does not allow discrimination
314 between $CCL3^{hi}$ vs. $CCL3^{low}$ GC B cells, the advantage that $CCL3^{hi}$ GC B cells may have
315 in contacting Tfr cells may be significantly underestimated and should be examined in
316 the future studies.
317
318 Tfr cells have been reported to control the size of GCs, to restrain participation of
319 bystander B cell clones in the GCs and development of anti-nuclear Ab responses, and
320 to increase the magnitude of foreign antigen-specific secondary Ab responses
321 (Alexander, Tygrett et al. 2011, Chung, Tanaka et al. 2011, Linterman, Pierson et al.
322 2011, Wollenberg, Agua-Doce et al. 2011, Wu, Chen et al. 2016, Botta, Fuller et al.
323 2017). In this work we found that B cell responses in CCL3-deficient mice mirror some of
324 those previously observed in mice with mislocalized or specifically ablated Tfr cells.
325 First, CCL3-KO mice generate slightly elevated GC responses following immunization.
326 Second, foreign Ag-specific secondary responses are reduced in CCL3-KO mice
327 compared to CCL3-proficient littermates. We also found that while foreign Ag specific

328 IgA responses in WT and CCL3-KO mice are comparable, total titers of IgA Abs in
329 immunized CCL3-KO mice are significantly elevated. Therefore, future studies should
330 examine whether CCL3 also contributes to better control over bystander or self-reactive
331 B cell clones in GCs and conveys better protection against development of
332 autoimmunity.
333
334 Interestingly, although CCL3 and CCL4 are coexpressed in activated and GC B cells,
335 neutralization of CCL4 at the time of GC formation did not promote significant increase in
336 the GC response in WT or CCL3-KO mice. It is possible that CCL4 expression in CCL3
337 KO cells is reduced as has been reported before (Patterson, Pesenacker et al. 2016).
338 Alternatively, CCL4 concentration produced by GC B cells is suboptimal for promotion of
339 Tfr cell response. CCL4 can be sensed through the G-protein coupled receptor CCR5,
340 while CCL3 may trigger both CCR5 and CCR1 receptors. Future studies should address
341 whether CCR5, CCR1, or both of these receptors are involved in the observed CCL3-
342 mediated regulation and interactions between GC B cells and Tfr cells.
343
344 While Tfr cells have been shown to control the numbers, specificity to foreign antigen
345 and cytokine production of Tfh cells that support GC responses *in vivo* (Sage, Francisco
346 et al. 2013, Sage, Paterson et al. 2014, Wing, Ise et al. 2014, Wu, Chen et al. 2016)
347 whether Tfr cells can directly affect GC B cells *in vivo* has not been definitively
348 demonstrated. Our *in vivo* data is consistent with a model of direct action of Tfr cells on
349 CCL3-secreting GC B cells. Depletion of regulatory T cells at the peak of the GC
350 response results in a relative increase in the numbers of CCL3-proficient, but not CCL3-
351 deficient HyHEL10 GC B cells. At the same time, during the resolution phase of GC
352 response CCL3-deficient HyHEL10 GC B cells are outcompeted by CCL3-proficient
353 HyHEL10 GC B cells and their participation in the PB response is reduced. Depletion of
354 Tregs at that time decreases the extent of CCL3-proficient GC B cell selection compared
355 to CCL3-deficient cells. Therefore, in addition to exerting a direct negative effect on B
356 cells in early GCs, Tfr cells also promote positive selection of CCL3-expressing GC B
357 cells at the later stages of the GC response. This scenario is consistent with deficiency
358 in secondary Ab responses in CCL3-KO mice observed in this study and previously
359 reported for Tfr cells-ablated mice (Linterman, Pierson et al. 2011). It is also consistent
360 with suggested positive role of Tfr cells-secreted IL10 for GC B cell selection (Laidlaw,

361 Lu et al. 2017). However, future studies should verify whether the observed direct effects
362 on GC B cells occur solely due to IL10 secretion by Tfr cells or whether multiple other
363 molecular players, including TGF-β, PD1, CTLA-4, GLUT1, and IL21 (Alexander, Tygrett
364 et al. 2011, Sage, Francisco et al. 2013, Sage, Paterson et al. 2014, Wing, Ise et al.
365 2014, Sage, Ron-Harel et al. 2016, Wu, Chen et al. 2016) may be involved. They should
366 also examine whether any additional mechanisms and cell types contribute to the
367 observed positive selection of CCL3-proficient GC B cells.
368
369 Previous intravital imaging studies of Tfh cell interactions with cognate GC B cells
370 revealed that majority of these encounters are transient (Allen, Okada et al. 2007).They
371 also suggested that a small fraction of the interactions that are more prolonged (> 5-10
372 min) may be more efficient for productive communication between the cells and for GC B
373 cell selection (Qi, Cannons et al. 2008, Shulman, Gitlin et al. 2014). In this study we
374 found that similarly to Tfh cells, a majority of interactions between foreign-antigen
375 specific GC B cells and natural Tfr cells *in vivo* are shorter than 5 min. Interestingly, Tfr
376 cells also formed a few interactions with GC B cells that were more prolonged. However,
377 while a few Tfh cell contacts with GC B exceeded 7.5 min, none of these have been
378 observed for Tfr cells. This discrepancy may be due to non-cognate interactions or very
379 weak cognate interactions between foreign antigen specific GC B cells and natural Tfr
380 cells. Future studies should directly address whether Tfr cells recognize MHCII/self-
381 peptides on GC B cells via T cell receptors (TCR), and how prevalent these cognate
382 interactions are. In addition, whether cognate interactions of Tfr cells with self antigen-
383 presenting GC B cells exert much stronger negative control of potentially self-reactive
384 GC B cells must be examined, as well as the contribution of CCL3 to that regulation.
385
386 In summary, our findings suggest that local CCL3 chemokine production by GC B cells
387 promotes their interactions with Tfr cells and plays a role in the optimal GC response.
388 Based on this data we suggest that local chemokine cues secreted by GC B cells may
389 be important in directing their interactions with other cell types and fine-tuning GC B cell
390 responses.
391
392
393

394 **MATERIALS AND METHODES**

395 **Mice, immunizations, and bone marrow chimeras**. C57BL/6 (B6, WT) mice were
396 purchased from the National Cancer Institute, Charles River or Jackson Laboratories.
397 B6-CD45.1 (002014), CCL3-KO (002687), β-actin-CFP (004218), UBC-GFP (004353),
398 Stop-tdTomato (007909) and E2a-Cre (003724) mice were from Jackson Laboratories.
399 HyHEL10 (Allen, Okada et al. 2007), MD4 (Goodnow, Crosbie et al. 1988), OTII
400 (Barnden, Allison et al. 1998), $Foxp3^{EGFP}$, and $Foxp3^{DTR}$ mice were from internal
401 colonies. All mice were housed in specific-pathogen free conditions. Relevant mice were
402 interbred to obtain HyHEL10 CFP^+, HyHEL10 GFP^+ CCL3-KO, OTII GFP^+, OTII
403 $tdTomato^+$, MD4 CFP^+, and $tdTomato^+$ $Foxp3^{EGFP}$ mice. 6-12 weeks old mice were
404 immunized s.c. with the protein antigens OVA (Sigma), DEL-OVA (produced as
405 previously described (Allen, Okada et al. 2007)), or NP-KLH (Biosearch Technologies),
406 mixed in either Ribi (Sigma) or Complete Freund Adjuvant (CFA, Sigma). In some
407 experiments 50 μg of anti-CCL4 (R&D clone 46907) or isotype control rat Abs (R&D
408 clone 54447) were s.c. administered into the preimmunized mice. All experiments were
409 performed in compliance with federal laws and institutional guidelines as approved by
410 the University Committee on Use and Care of Animals.
411

412 **Cell isolation, flow cytometry analysis and cell sorting.** Lymphocytes were isolated
413 by homogenizing lymph nodes (LNs) and/or spleens into a single cell suspension in
414 DMEM medium (Corning) containing 2% fetal bovine serum (FBS, Atlanta Biologicals),
415 antibiotics (50 IU/mL of penicillin and 50 *μ*g/mL of streptomycin; Gibco) and 10 mM
416 HEPES (Gibco) and straining through a 70 *μ*m mesh filter (Falcon) in the presence of 20
417 *μ*g/ml of DNase I (Sigma-Aldrich). Red blood cells were lysed using Tris-buffered NH_4Cl.
418 The following antibodies and reagents were used for flow cytometry analysis: CD3 (BD,
419 145-2C11), CD4 (BD, RM4-5), CD8 (BD, 53-6.7), CD25 (BD, PC61.5), B220 (BD, RA3-
420 6B2), CD19 (BD, 1D3), CXCR5 (BD, 2G8), Fas (BD, Jo2), IgM (BD, R6-60.2), IgM^a (BD,
421 DS-1), Vβ5 (BD, MR9-4), CD43 (BD, S7), CD19 (Biolegend, 6D5), CD45.1 (Biolegend,
422 A20), CD45.2 (Biolegend, 104), IgD (Biolegend, 11-26c.2a), PD-1 (Biolegend, RMP1-
423 30), CXCR4 (eBiosciences, 2B11), CD86 (Biolegend, GL1), Foxp3 (eBiosciences, FJK-
424 16s), GL-7 (eBiosciences, GL-7), SA-qDot607 (Life Technologies), SA-DyLight 488
425 (Biolegend). Single-cell suspensions were incubated with biotinylated antibodies for 20

426 minutes on ice, washed twice with 200 μl PBS supplemented with 2% FBS, 1 mM EDTA,
427 and 0.1% NaN (FACS buffer), and then incubated with fluorophore-conjugated
428 antibodies and streptavidin for 20 minutes on ice, and washed twice more with 200 μl
429 FACS buffer. For FoxP3 staining the cells were permeabilized and stained using FoxP3
430 staining buffer set (eBioscience) according to the manufacturer's instructions. Cells were
431 then resuspended in FACS buffer for acquisition. All flow cytometry analyses and cell-
432 sorting procedures were done using FACSCanto II and FACSAria IIIu respectively.
433 FlowJo Software (v 9.7; TreeStar) was used for data analyses and plot rendering.
434
435 **Cell purification and adoptive transfers**. For adoptive transfers, cells were isolated
436 from combined spleens and LNs of donor mice and CD4 T cells or B cells were enriched
437 using autoMACS (Miltenyi Biotec) as described before (Allen, Okada et al. 2007). The
438 purity of B cells was >95%, and CD4 T cells >70% for all experiments. Lymphocytes
439 were adoptively transferred by intravenous injection into the lateral tail vein.
440
441 **Generation of mice with Tregs and Tfr cells expressing tdTomato.** In order to
442 generate mice with fluorescent Tregs the following scheme was utilized: first, tdTomato
443 expressing mice were crossed with Foxp3^{EGFP} mice. Second, tdTomato^{+}Foxp3^{EGFP} Tregs
444 were sorted and adoptively transferred into Foxp3^{DTR} mice where endogenous Tregs
445 were transiently ablated by DTx treatment (Sigma). To sort tdTomato expressing Tregs,
446 the LNs and spleens from the tdTomato^{+}Foxp3^{EGFP} mice were combined and lymphocyte
447 suspension was prepared as described above. The lymphocytes were separated from
448 RBCs using Ficoll-Paque (GE Healthcare) gradients per manufacturer's instructions
449 using 14 mL round bottom tubes (Falcon). Single cell suspensions were enriched for
450 CD4^{+} T cells as described above. Following the enrichment, EGFP^{+} cells were sorted
451 into DMEM medium supplemented with 10% FCS. The purity of sorted Tregs as
452 determined by intracellular Foxp3 staining was > 99%. About 0.8-1.5 million of purified
453 tdTomato^{+} Tregs were then transferred into recipient Foxp3^{DTR} mice via tail vein injection.
454 Finally, one day later the endogenous nonfluorescent Tregs in the recipient Foxp3^{DTR}
455 mice were ablated by intraperitoneal injection of 5 μg/kg of DTx in PBS. The DTx
456 treatment was repeated once more a week later.
457

458 **Cell culture and chemotaxis.** Transwells with 5 μm pore size (Corning) were used.
459 CD4 T cells were isolated and enriched as described above from draining peripheral LNs
460 of mice s.c. immunized with OVA in Ribi at 10 days following immunization. T cells were
461 resuspended with RPMI 1640 (Corning) supplemented with 2% fatty acid free BSA
462 (Sigma-Aldrich), 10 mM HEPES, 50 IU/mL of penicillin, and 50 mg/mL of streptomycin
463 (HyClone). For chemotaxis analysis the lower chambers of transwells were filled with the
464 same medium mixed with various concentrations of CCL3 or CCL4 chemokines
465 (PeproTech). For chemokinesis analysis both upper and lower chambers of transwells
466 were filled with either 200 ng/mL of CCL3 or with 400 ng/mL CCL4. Transwells with
467 chemokines and resuspended CD4 T cells were incubated at 37ºC and 5% CO_2 for 10
468 minutes. After that, CD4 T cells were placed in the upper chambers of transwells at
469 $4x10^5$ cells per well and incubated at 37ºC and 5% CO_2 for 3 hours. Two to three
470 replicas per condition have been performed per experiment. The transmigrated fraction
471 of cells was stained and analyzed via flow cytometry. Chemotactic index was calculated
472 as the ratio of cells that transmigrated to chemokine compared to no cytokine control.
473
474 **Enzyme-linked immunosorbent assay.** For measuring NP-specific Abs, NUNC
475 immunoplates were coated with 2 µg/mL of NP2-BSA or NP30-BSA (Biosearch) in
476 borate saline buffer (100mM boric acid, pH 7.4, 0.9% NaCl). For measuring total titers of
477 IgA, IgG1, IgG2b and IgG2c, plates were coated with 4 µg/mL of purified goat anti-
478 mouse Ig (H+L) (Southern Biotech, cat #1010-01). Blocking was done with PBS
479 containing 0.1% gelatin and 0.1% sodium azide. Washes were done with PBS containing
480 0.05% Tween-20. Serial serum dilutions were applied. For detection of IgA, IgG1, and
481 IgG2b, the plates were incubated with 1:4000 dilution of biotinylated mouse anti-mouse
482 IgA, IgG1, and rat anti-mouse IgG2b (BD Biosciences, clones C10-1, 10.9, and R12-3)
483 respectively followed by streptavidin-HRP (R&D). The color was developed using a
484 substrate solution from R&D (DY999). For detection of IgG2c the plates were incubated
485 with AP-conjugated goat anti-mouse IgG2c Abs (Southern Biotech, cat #1079-04) and
486 visualized by incubating with nitrophenyl phosphate (Sigma) in carbonate buffer (22 mM
487 Sodium carbonate, 34 mM sodium bicarbonate, 2.1 mM MgCl2). Plates were read with a
488 Synergy HT microplate reader (Bio-Tek Incorporated) at 405 and 562 nm. All plates
489 contained serial dilutions of the serum that was used to generate the calibration curve for
490 quantitative comparison of the samples.

491 **Two Photon Microscopy.** Inguinal LNs (ILNs) were either explanted or surgically
492 exposed for intravital imaging and perfused as previously described (Allen, Okada et al.
493 2007, Grigorova, Schwab et al. 2009). ILNs were imaged with a Leica SP5 II (Leica
494 Microsystems) fitted with a MaiTai Ti:Sapphire laser (Sepctra-Physics) that was tuned to
495 870 nm. Each *xy* plane spanned 435 μm x 435 μm and with z spacing ranging from 2-3
496 μm detecting emission wavelengths of 430-450 nm (second harmonic emission of
497 collagen), 465-500 nm (for CFP^+ cells), 520-550 nm (for GFP^+ cells), and >560 nm (for
498 $tdTomato^+$ cells), every 20-25 seconds. Images were acquired by Leica Advanced
499 Fluorescent Suite (Leica Microsystems). Analysis of the imaging data and generation of
500 3D rotations and time-lapse image sequences were performed using Imaris 7.6.5 x 64
501 (Bitplane). Videos were processed with a median noise filter. Semi-automated cell
502 tracking in 3D was performed with Imaris 7.6.5 x 64, and then verified and corrected
503 manually. 3-dimensional GC volume was defined based on the distribution of HyHEL10
504 CFP B cells by combination of visual analysis and a custom-made MATLAB program
505 that performed time integrated image rendering of CFP signal. $TdTomato^+$ Tregs and Th
506 that transited within the follicles and GCs were tracked. Their interaction with WT and
507 CCL3-KO B cells within defined GCs volume were visually identified and categorized
508 either as a strict contact as defined when cell-to-cell contact was unambiguous or a non-
509 strict contacts where cells could be observed in extreme proximity (~1 μm). Finally, we
510 normalized the number of contacts to the average number of WT or CCL3-KO B cells
511 within the GC volume accessible to Tfr or Tfh cells to arrive at a normalized contact
512 frequency. Annotation and final compilation of videos was performed in Adobe After
513 Effects CS5.5 (Adobe).
514
515 **RT-PCR Analysis**. RNA from sorted cells was obtained using RNeasy Kit (Qiagen)
516 following the manufacturer's instructions. RNA was treated with DNase to remove
517 genomic DNA (Ambion). The concentration of RNA was calculated using a NanoDrop
518 2000 (Thermo) and cDNA was synthesized using a SuperScript III kit (Invitrogen)
519 following the manufacturer's instructions. Preamplification of target genes was performed
520 using PreAmp Kit (AB Biosystems) for 10 cycles. TaqMan assays were obtained from
521 Applied Biosystems and RT-PCR was carried out on a RealPlex 2 (Eppendorf).
522 Expression levels of CCL3/4 were normalized to the level of β2m.
523

524 **Single cell RT-PCR Analysis.** Single cell RT-PCR was performed using the method
525 described before (Wang and Janes 2013). In brief, mice were s.c. immunized with OVA
526 in Ribi and dLNs were collected at 10 d.p.i. GC CC and CB were sorted as described in
527 **Fig. 1a**. Naive (non-GC B cells) were sorted as $B220^{+}CD3^{-}FAS^{low}GL7^{low}$ cells. RNA from
528 sorted cells was obtained by sorting single cells directly into 3.6 mL of predigestion
529 buffer (1.1 μL Invitrogen 5x First Strand Buffer, 4 mM dNTP, 2.74 mL nuclease free
530 H_2O). Cells were freeze thawed and 0.4 mL of digestion buffer was added (1% w/v
531 saponin (Sigma Aldrich), 25 mg/mL proteinase K (Sigma Aldrich)) and the total volume
532 was transfered to 1.5 mL tubes and incubated at 42° C for 1 hour. Digestion was stopped
533 by adding 1 mL of STOP buffer (20 U/mL anti-RNase (Ambion), 20 U/mL SUPERase-IN
534 (Ambion), 100 mM PMSF (Sigma Aldrich)). The volume was transferred to a 96-well
535 plate and 0.5 mL of Invitrogen SuperScript III was added to each well. The plate was
536 incubated at 50° C for 15 minutes and RT was deactivated by incubating at 70° C for 15
537 minutes. Samples were spun down and 1mL of RNaseH (Invitrogen) in a solution of 12.5
538 mM $MgCl_2$ was added and incubated at 37° C for 15 minutes. Samples were spun down
539 and 3.5 mL of tailing buffer with 0.2 mL of TdT (Roche) was added (363 mL H_2O, 400 μL
540 Invitrogen 5x TdT buffer, 15 μL 100 mM dATP). Samples were incubated at 37° C for 15
541 minutes than heat inactivated by incubating at 65° C for 10 minutes. Samples were spun
542 and preamplification via PCR was done with the following mix by adding 40 μL to each
543 sample: 5 μL of 10x ThermoPol (NEB), 1.25 μL 100 mM MgSO4, 0.25 μL 20 mg/ml BSA,
544 5 μL 10 mM dNTP, 1 μL AmpliTaq Gold (Applied Biosystems), 0.9 μL of 15 μg/mL AL1
545 primer (IDT): ATTGGATCCAGGCCGCTCTGGACAAAATATGAATTCTTTTTTTTTTTT
546 TTTTTTTTTTTT, and 26.6 μL of H_2O. Reaction conditions were as follows: cycles 1-4
547 94° C for 1 minute, 32° C for 2 minutes, and 72° C for 6 minutes with 10 second
548 increases to elongation in each cycle. Cycles 5-25, 94° C for 1 minute, 42° C for 2
549 minutes, and 72° C for 6 minutes and 40 seconds with 10 second increases to elongation
550 each cycle. Cycles 26 - 35: 94° C for 1 minute, 42° C for 2 minutes, and 72° C for 6
551 minutes. qPCR was than performed on 1 μL of template DNA by using gene specific
552 primers and POWER SYBER Green (Applied Biosystems) and following the
553 manufacturer's supplied directions. Sequences are as follows: B2m.S:
554 ATGCCAAACCCTCTGTACTTCT, B2m.as: ATTGGGCACAGTGACAGACT, HPRT1.s:
555 ACGAGTCTGAAGCTCTCGATTT, HPRT1.as: CAGCCAACACTGCTGAAACAT,

556 CCL3.s: TCCATGGGTCCCGTGTAGAG, CCL3.as: GTGGCTACTTGGCAGCAAAC,
557 CCL4.s: GTGCTAACCCCAGTGAGCC, CCL4.as: GAGCAAGGACGCTTCTCAGT. A
558 melting curve was done following amplification. Cells were excluded from analysis if they
559 failed to give a single product or did not amplify at the same rate. Cells were also
560 excluded if they do not amplify, CCL3, CCL4, B2m, and HPRT1.
561
562 **Statistical analysis.** All statistical tests were computed with PRISM (GraphPad) after
563 consultation with a University of Michigan Center for Statistical Consultation and
564 Research representative. Statistical analysis of data normalized to the control samples
565 were performed using a one-sample *t*-test. For comparisons between two groups *t*-test
566 was utilized. Welch's correction was applied for data with unequal variances. For data in
567 which more than two groups or more than two time points were analyzed, two-way
568 ANOVA followed by Dunnet post-hoc analysis was done. In cases where we did not
569 assume normally distributed data and the data was from paired measurements, we used
570 the Wilcoxon signed-rank test. The analysis of the CCL3/4 single cell expression data
571 was performed using Maximal Likelihood Estimation method. The data was fit to k=1:5
572 Gaussian distributions using Matlab function gmdistribution.fit. The goodness of fit to
573 single or more distributions was calculated using the negative log likelihoods.
574 Significance was determined by comparing the ratio of the fits to the χ^2 distribution.
575 *P* values of less than 0.05 were considered statistically significant. All statistically
576 significant results were labeled. No samples were excluded from the analysis.
577
578 **AUTHOR CONTRIBUTIONS**
579 Z.L.B. planned, performed and analyzed experiments and prepared the manuscript;
580 F.K., M.M., R.W. and J.S.T. helped with various aspects of other experiments; J.B.G.,
581 M.I.I., and S.S.S. performed blind analysis of the imaging data; I.G. planned, performed
582 and analyzed experiments, and prepared the manuscript.
583
584 **ACKNOWLEDGMENTS**
585 We thank W. Dunnick and E. Perkey for discussions; J. Cyster (University of California
586 San Francisco), W. Zhou (University of Michigan Medical school), and A. Rudensky
587 (Memorial Sloan Kettering Cancer Center) for provision of mice; the University of
588 Michigan flow cytometry core for cell sorting assistance. Supported by the American

Heart Association (14PRE19960005) to Z.B., by the Herman and Dorothy Miller Award for Innovative Immunology Research to J.S.T. and Z.L.B., and National Institute of Health (R01 AI106806) to I.G. The authors declare no competing financial interests.

622 **REFERENCES**

623 Alexander, C. M., L. T. Tygrett, A. W. Boyden, K. L. Wolniak, K. L. Legge and T. J.
624 Waldschmidt (2011). "T regulatory cells participate in the control of germinal centre
625 reactions." Immunology **133**(4): 452-468.
626 Allen, C. D., T. Okada and J. G. Cyster (2007). "Germinal-center organization and
627 cellular dynamics." Immunity **27**(2): 190-202.
628 Allen, C. D., T. Okada, H. L. Tang and J. G. Cyster (2007). "Imaging of germinal center
629 selection events during affinity maturation." Science **315**(5811): 528-531.
630 Aloulou, M., E. J. Carr, M. Gador, A. Bignon, R. S. Liblau, N. Fazilleau and M. A.
631 Linterman (2016). "Follicular regulatory T cells can be specific for the immunizing
632 antigen and derive from naive T cells." Nat Commun **7**: 10579.
633 Barnden, M. J., J. Allison, W. R. Heath and F. R. Carbone (1998). "Defective TCR
634 expression in transgenic mice constructed using cDNA-based alpha- and beta-chain
635 genes under the control of heterologous regulatory elements." Immunol Cell Biol **76**(1):
636 34-40.
637 Bettelli, E., Y. Carrier, W. Gao, T. Korn, T. B. Strom, M. Oukka, H. L. Weiner and V. K.
638 Kuchroo (2006). "Reciprocal developmental pathways for the generation of pathogenic
639 effector TH17 and regulatory T cells." Nature **441**(7090): 235-238.
640 Botta, D., M. J. Fuller, T. T. Marquez-Lago, H. Bachus, J. E. Bradley, A. S. Weinmann,
641 A. J. Zajac, T. D. Randall, F. E. Lund, B. Leon and A. Ballesteros-Tato (2017). "Dynamic
642 regulation of T follicular regulatory cell responses by interleukin 2 during influenza
643 infection." Nat Immunol **18**(11): 1249-1260.
644 Bystry, R. S., V. Aluvihare, K. A. Welch, M. Kallikourdis and A. G. Betz (2001). "B cells
645 and professional APCs recruit regulatory T cells via CCL4." Nat Immunol **2**(12): 1126-
646 1132.
647 Caron, G., S. Le Gallou, T. Lamy, K. Tarte and T. Fest (2009). "CXCR4 expression
648 functionally discriminates centroblasts versus centrocytes within human germinal center
649 B cells." J Immunol **182**(12): 7595-7602.
650 Chung, Y., S. Tanaka, F. Chu, R. I. Nurieva, G. J. Martinez, S. Rawal, Y. H. Wang, H.
651 Lim, J. M. Reynolds, X. H. Zhou, H. M. Fan, Z. M. Liu, S. S. Neelapu and C. Dong
652 (2011). "Follicular regulatory T cells expressing Foxp3 and Bcl-6 suppress germinal
653 center reactions." Nat Med **17**(8): 983-988.
654 Compagno, M., W. K. Lim, A. Grunn, S. V. Nandula, M. Brahmachary, Q. Shen, F.
655 Bertoni, M. Ponzoni, M. Scandurra, A. Califano, G. Bhagat, A. Chadburn, R. Dalla-

656 Favera and L. Pasqualucci (2009). "Mutations of multiple genes cause deregulation of
657 NF-kappaB in diffuse large B-cell lymphoma." Nature **459**(7247): 717-721.
658 Cook, D. N., M. A. Beck, T. M. Coffman, S. L. Kirby, J. F. Sheridan, I. B. Pragnell and O.
659 Smithies (1995). "Requirement of MIP-1 alpha for an inflammatory response to viral
660 infection." Science **269**(5230): 1583-1585.
661 Fu, W., X. Liu, X. Lin, H. Feng, L. Sun, S. Li, H. Chen, H. Tang, L. Lu, W. Jin and C.
662 Dong (2018). "Deficiency in T follicular regulatory cells promotes autoimmunity." J Exp
663 Med **215**(3): 815-825.
664 Goodnow, C. C., J. Crosbie, S. Adelstein, T. B. Lavoie, S. J. Smith-Gill, R. A. Brink, H.
665 Pritchard-Briscoe, J. S. Wotherspoon, R. H. Loblay, K. Raphael and et al. (1988).
666 "Altered immunoglobulin expression and functional silencing of self-reactive B
667 lymphocytes in transgenic mice." Nature **334**(6184): 676-682.
668 Green, J. A., K. Suzuki, B. Cho, L. D. Willison, D. Palmer, C. D. Allen, T. H. Schmidt, Y.
669 Xu, R. L. Proia, S. R. Coughlin and J. G. Cyster (2011). "The sphingosine 1-phosphate
670 receptor S1P(2) maintains the homeostasis of germinal center B cells and promotes
671 niche confinement." Nat Immunol **12**(7): 672-680.
672 Grigorova, I. L., S. R. Schwab, T. G. Phan, T. H. Pham, T. Okada and J. G. Cyster
673 (2009). "Cortical sinus probing, S1P1-dependent entry and flow-based capture of
674 egressing T cells." Nat Immunol **10**(1): 58-65.
675 Kim, J. M., J. P. Rasmussen and A. Y. Rudensky (2007). "Regulatory T cells prevent
676 catastrophic autoimmunity throughout the lifespan of mice." Nat Immunol **8**(2): 191-197.
677 Krzysiek, R., E. A. Lefevre, W. Zou, A. Foussat, J. Bernard, A. Portier, P. Galanaud and
678 Y. Richard (1999). "Antigen receptor engagement selectively induces macrophage
679 inflammatory protein-1 alpha (MIP-1 alpha) and MIP-1 beta chemokine production in
680 human B cells." J Immunol **162**(8): 4455-4463.
681 Laidlaw, B. J., Y. Lu, R. A. Amezquita, J. S. Weinstein, J. A. Vander Heiden, N. T.
682 Gupta, S. H. Kleinstein, S. M. Kaech and J. Craft (2017). "Interleukin-10 from CD4(+)
683 follicular regulatory T cells promotes the germinal center response." Sci Immunol **2**(16).
684 Liang, W. G., C. G. Triandafillou, T. Y. Huang, M. M. Zulueta, S. Banerjee, A. R. Dinner,
685 S. C. Hung and W. J. Tang (2016). "Structural basis for oligomerization and
686 glycosaminoglycan binding of CCL5 and CCL3." Proc Natl Acad Sci U S A **113**(18):
687 5000-5005.

688 Lim, H. W., P. Hillsamer, A. H. Banham and C. H. Kim (2005). "Cutting edge: direct
689 suppression of B cells by CD4+ CD25+ regulatory T cells." J Immunol **175**(7): 4180-
690 4183.
691 Linterman, M. A., W. Pierson, S. K. Lee, A. Kallies, S. Kawamoto, T. F. Rayner, M.
692 Srivastava, D. P. Divekar, L. Beaton, J. J. Hogan, S. Fagarasan, A. Liston, K. G. Smith
693 and C. G. Vinuesa (2011). "Foxp3+ follicular regulatory T cells control the germinal
694 center response." Nat Med **17**(8): 975-982.
695 Maurer, M. and E. von Stebut (2004). "Macrophage inflammatory protein-1." Int J
696 Biochem Cell Biol **36**(10): 1882-1886.
697 Menten, P., A. Wuyts and J. Van Damme (2002). "Macrophage inflammatory protein-1."
698 Cytokine Growth Factor Rev **13**(6): 455-481.
699 Patterson, S. J., A. M. Pesenacker, A. Y. Wang, J. Gillies, M. Mojibian, K. Morishita, R.
700 Tan, T. J. Kieffer, C. B. Verchere, C. Panagiotopoulos and M. K. Levings (2016). "T
701 regulatory cell chemokine production mediates pathogenic T cell attraction and
702 suppression." J Clin Invest **126**(3): 1039-1051.
703 Pereira, J. P., L. M. Kelly, Y. Xu and J. G. Cyster (2009). "EBI2 mediates B cell
704 segregation between the outer and centre follicle." Nature **460**(7259): 1122-1126.
705 Qi, H., J. L. Cannons, F. Klauschen, P. L. Schwartzberg and R. N. Germain (2008).
706 "SAP-controlled T-B cell interactions underlie germinal centre formation." Nature
707 **455**(7214): 764-769.
708 Sage, P. T., L. M. Francisco, C. V. Carman and A. H. Sharpe (2013). "The receptor PD-1
709 controls follicular regulatory T cells in the lymph nodes and blood." Nat Immunol **14**(2):
710 152-161.
711 Sage, P. T., A. M. Paterson, S. B. Lovitch and A. H. Sharpe (2014). "The coinhibitory
712 receptor CTLA-4 controls B cell responses by modulating T follicular helper, T follicular
713 regulatory, and T regulatory cells." Immunity **41**(6): 1026-1039.
714 Sage, P. T., N. Ron-Harel, V. R. Juneja, D. R. Sen, S. Maleri, W. Sungnak, V. K.
715 Kuchroo, W. N. Haining, N. Chevrier, M. Haigis and A. H. Sharpe (2016). "Suppression
716 by TFR cells leads to durable and selective inhibition of B cell effector function." Nat
717 Immunol **17**(12): 1436-1446.
718 Shulman, Z., A. D. Gitlin, J. S. Weinstein, B. Lainez, E. Esplugues, R. A. Flavell, J. E.
719 Craft and M. C. Nussenzweig (2014). "Dynamic signaling by T follicular helper cells
720 during germinal center B cell selection." Science **345**(6200): 1058-1062.

721 Victora, G. D., D. Dominguez-Sola, A. B. Holmes, S. Deroubaix, R. Dalla-Favera and M.
722 C. Nussenzweig (2012). "Identification of human germinal center light and dark zone
723 cells and their relationship to human B-cell lymphomas." Blood **120**(11): 2240-2248.
724 Wang, L. and K. A. Janes (2013). "Stochastic profiling of transcriptional regulatory
725 heterogeneities in tissues, tumors and cultured cells." Nat Protoc **8**(2): 282-301.
726 Wing, J. B., W. Ise, T. Kurosaki and S. Sakaguchi (2014). "Regulatory T cells control
727 antigen-specific expansion of Tfh cell number and humoral immune responses via the
728 coreceptor CTLA-4." Immunity **41**(6): 1013-1025.
729 Wing, J. B. and S. Sakaguchi (2014). "Foxp3(+) T(reg) cells in humoral immunity." Int
730 Immunol **26**(2): 61-69.
731 Wollenberg, I., A. Agua-Doce, A. Hernandez, C. Almeida, V. G. Oliveira, J. Faro and L.
732 Graca (2011). "Regulation of the germinal center reaction by Foxp3+ follicular regulatory
733 T cells." J Immunol **187**(9): 4553-4560.
734 Wu, H., Y. Chen, H. Liu, L. L. Xu, P. Teuscher, S. Wang, S. Lu and A. L. Dent (2016).
735 "Follicular regulatory T cells repress cytokine production by follicular helper T cells and
736 optimize IgG responses in mice." Eur J Immunol **46**(5): 1152-1161.

737
738
739
740
741
742
743
744
745
746
747
748
749
750
751
752
753

754 **FIGURES**

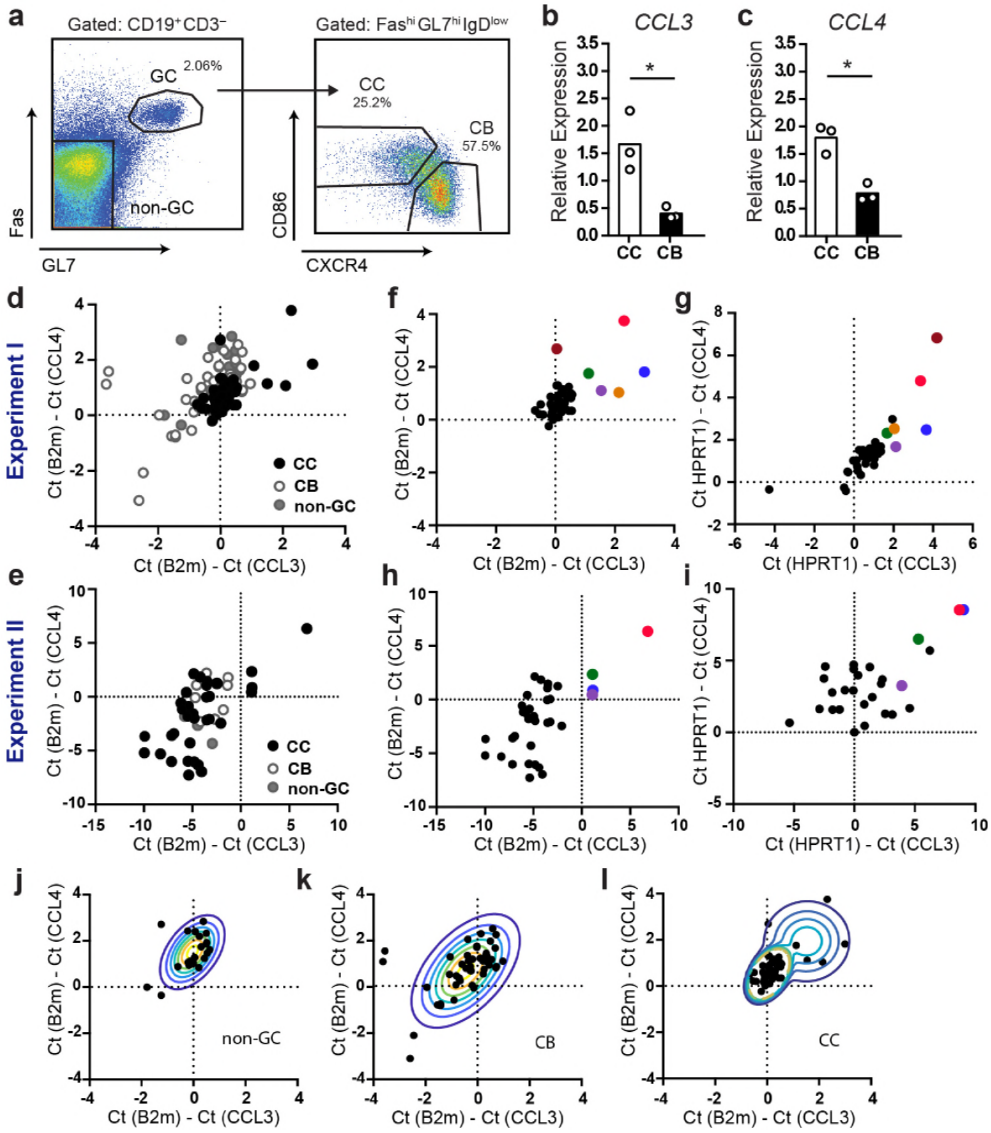

755

756 **Figure 1. A small subset of GC centrocytes upregulates CCL3/4 expression**. qRT-PCR
757 analysis of CCL3 and CCL4 expression in GC and non-GC B cells sorted from the draining LNs of
758 mice s.c. immunized with 50 μg ovalbumin (OVA) in Ribi at 10 days post immunization (d.p.i). **a**,
759 The gating strategy for cell sorting. **b, c**, Relative expression of CCL3/4 in bulk GC centroblasts
760 (CB) and centrocytes (CC) as normalized to non-GC B cells (FAS^{low} $GL7^{low}$). Chemokine C_T
761 values were normalized to β2m C_T. Bars represent mean with dots representing average values
762 per experiment. Data represent n=3 independent experiments, 4 mice total. *, P<0.05, two-tailed
763 Student's *t*-test. **d-l**, Single cell qPCR analysis of B cells sorted as indicated in a. **d**,**e**, Overlay of
764 CC, CB and non-GC B cells' CCL3/4 expression data. 2 independent experiments. Cells
765 expressing the highest levels of CCL3/4 are located in the top right quadrant. **f-i**, Elevated
766 expression of CCL3/4 in a subset of GC CC is independent of B2M (f, h) or HPRT1 (g, h) Ct used
767 for normalization. Same cells are labeled in the same colors in experiment I (f, g) or II (h, i). **j-l**,
768 Density plots illustrate Gaussian distributions, that provided the best fit for the expression data:
769 one for non-GC B cells (j) and CB (k) or two for CC(l). The contours are based on the underlying
770 probability distribution function for the data and were generated in MATLAB Software using
771 gmdistribution.fit and then fcontour functions.

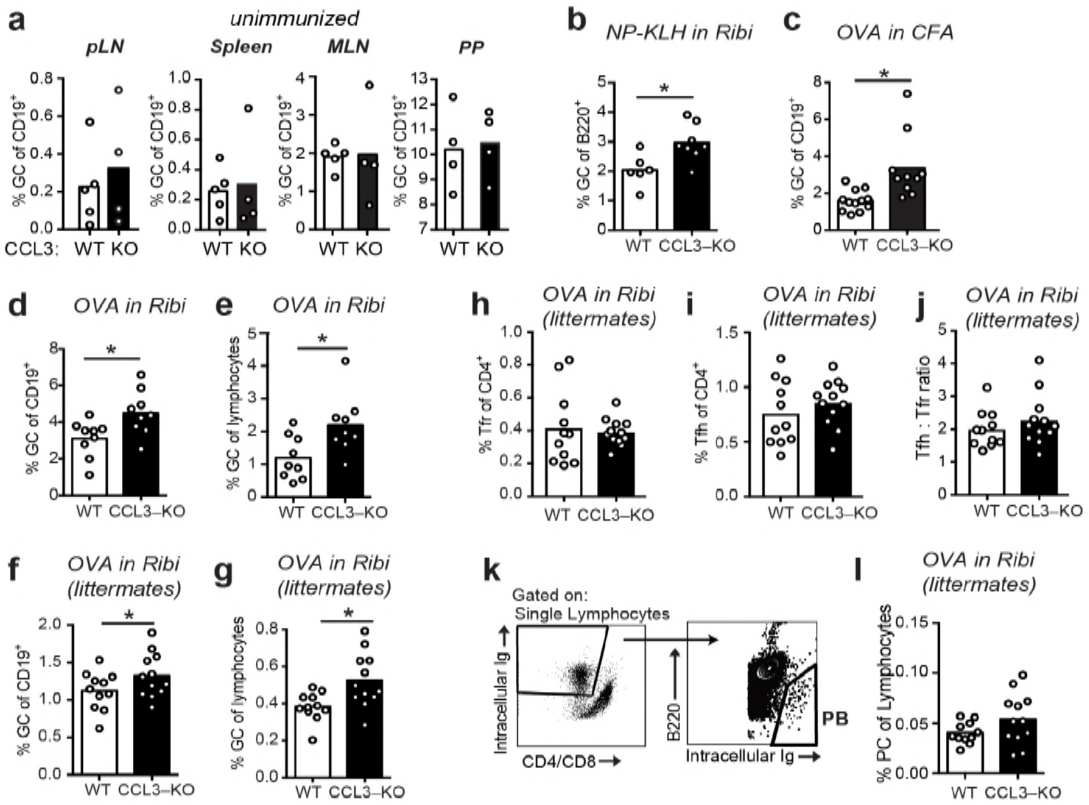

Figure 2. Increased GC response in CCL3-KO mice following immunization. **a-g**, Flow cytometry analysis of the GC B cells (Fas^{high} GL7^{high} IgD^{low}) as a fraction of total B cells (a-d, f) or total lymphocytes (e, g) in WT and CCL3-KO mice. **a**, Analysis of GCs in pLNs (inguinal, brachial and auxillary LNs combined), spleens, MLNs, and PP from unimmunized mice. **b-g**, Analysis of GCs in the dLNs from mice s.c. immunized with 50 μg of 4-Hydroxy-3-nitrophenyl (*NP*) acetyl-*hapten* conjugated to *Keyhole limpet hemocyanin (*KLH) in Ribi adjuvant (b) or 50 μg of OVA in Complete Fruend's Adjuvant (CFA) (c) or 50 μg OVA in Ribi (d-g) at 10 d.p.i. **f-l,** Flow cytometry analysis of GC (f, g), Follicular T cell (h-j), and plasma cell (PC) (k, l) response in dLNs of WT and CCL3-KO littermate conrol mice s.c. immunized with 50 μg OVA in Ribi at 10 d.p.i. **h-j**, Tfr (CXCR5^{high} PD1^{high} FoxP3^{pos} in h) and Tfh (CXCR5^{high} PD1^{high} FoxP3^{neg} in i) cells as a fraction of CD4 T cells. **k, l**, PB gating strategy (k) and PBs as a fraction of total lymphocytes (l). Each symbol represents one mouse. Bars represent mean. Data are derived from 2 or 3 independent experiments. *, P<0.05, Student's *t*-test (two-sided in b-e, one-sided in f, g).

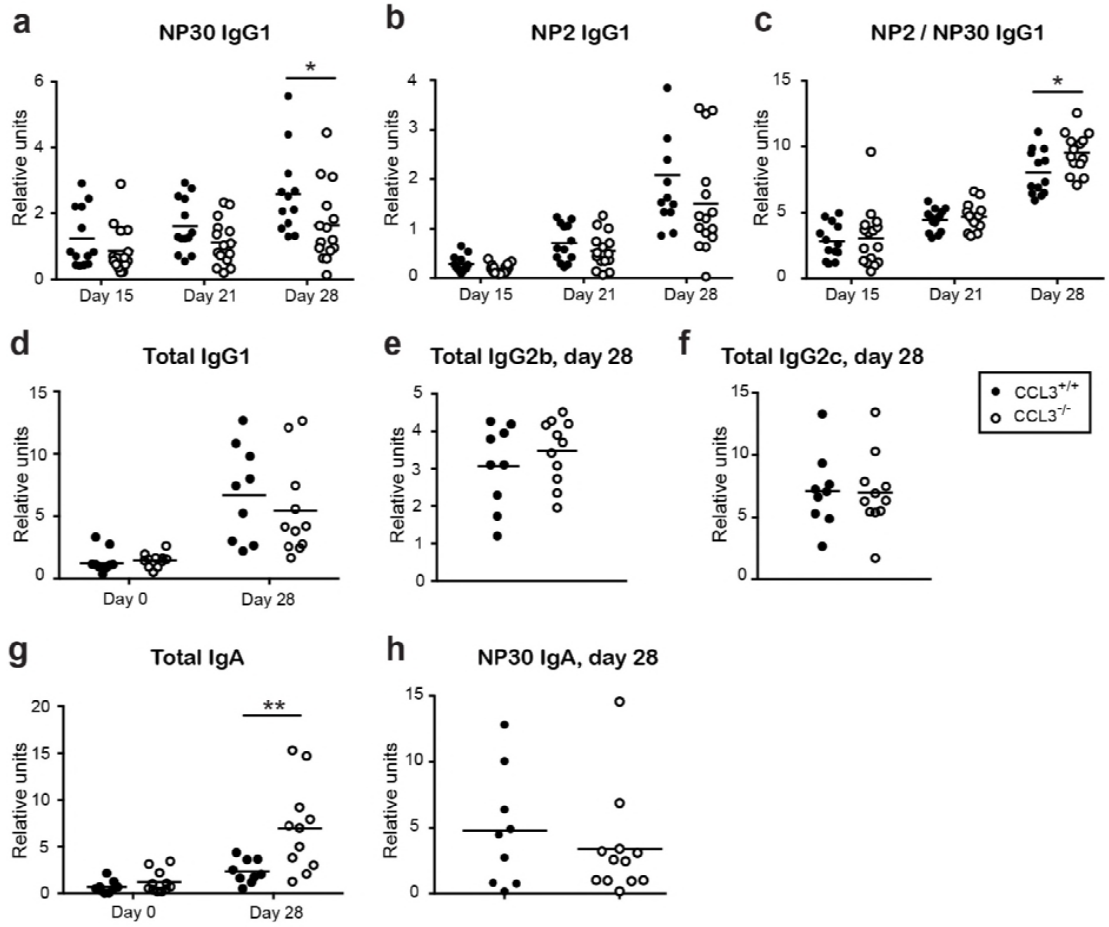

Figure 3. Foreign Ag-specific Ab response in CCL3-KO mice. a-e, Analysis of serum from WT (black circles) and CCL3-KO (white circles) littermate control mice s.c. immunized with 50 μg of NP-KLH in Ribi and boosted with the same dose of antigen in Ribi on day 24 by ELISA and bled on 0, 15, 21, 28 d.p.i. **a-c,** Analysis of NP30-specific IgG1 (in a), NP2-specific high-affinity IgG1 (in b), and NP2/NP30 IgG1 ratio (in c). **d-g**, Analysis of total IgG1 (in d), IgG2b (in e), IgG2c (in f), and IgA (in g) Abs. **e**, Analysis of NP-30 specific IgA Abs. Relative titers were determined using serial dilutions and a calibration curve from control serum. Data represents 3 (in d-h) or 4 (in a-c) independent experiments. Each symbol represents one mouse. Lines represent mean. *, $P<0.05$, **, $P<0.01$. Two-tailed Student's t-test.

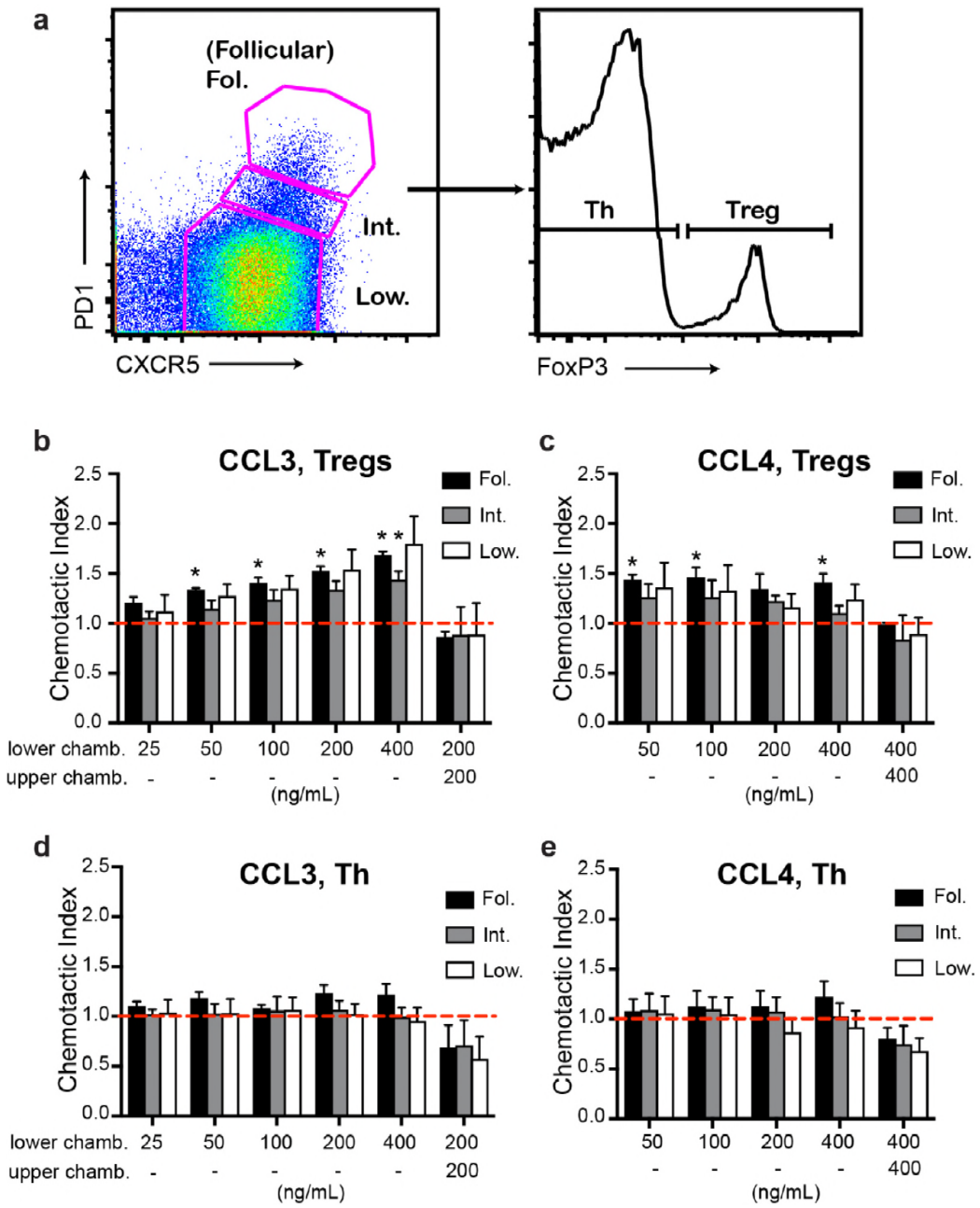

Figure 4. **Chemotaxis of Tfr cells to CCL3 and CCL4 *ex vivo*. a-e,** *Ex vivo* transwell assay of $CD4^+$ T cells purified from dLNs of WT mice at 10 d.p.i. with 100 μg OVA in Ribi and analyzed by flow cytometry using the gating strategy as in (a). Transmigration of $CXCR5^{high}PD1^{high}$ (Fol., black bars), $CXCR5^{int}PD^{int}$ (Int., grey bars), or $CXCR5^{low}PD1^{low}$ (Low, white bars) $CD4^{pos}$ $CD8^{neg}$ B220 ^{neg} cell populations that also express Foxp3 (b, c) or were FoxP3 ^{neg} (d, e) were measured against CCL3 (b, d) and CCL4 (c, e). The chemokines were added either to the lower chambers (chamb.) of transwells for analysis of chemotaxis or to both the upper and the lower chambers for analysis of chemokinesis. Chemotactic index was calculated as the ratio of cells that transmigrated towards the chemokine vs. no chemokine control (dashed red line). Chemotaxis and chemokinesis data are derived from 3 and 2 independent experiments correspondingly with 2 mice per experiment. Bars represent mean ± SEM, *, P<0.05, two-tailed, one-sample Student's *t*-test (compared to 1).

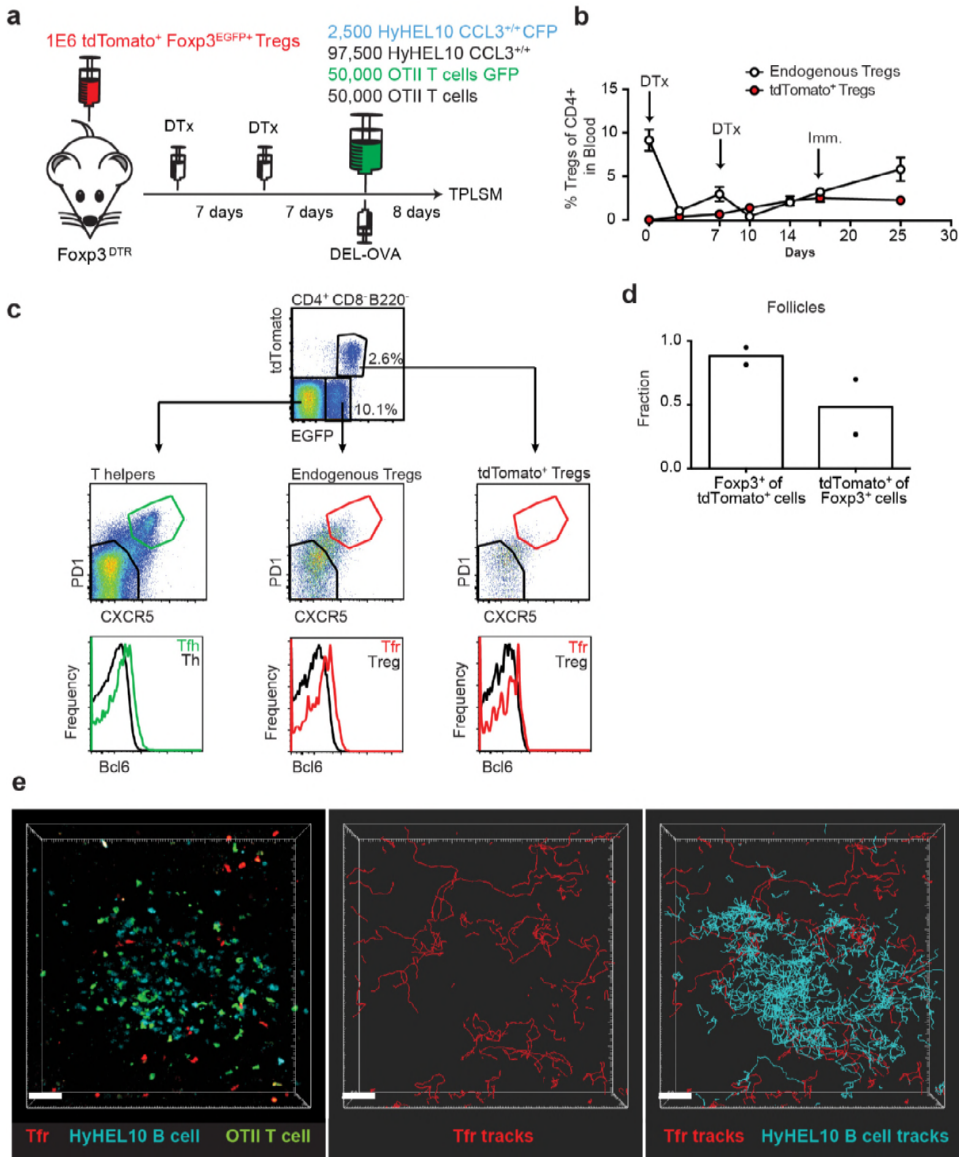

Figure 5. 2P visualization of Tfr cells and HyHEL10 GC B cells. a, Experimental diagram for generation of recipient mice with large numbers of highly fluorescent tdTomato^{+} Tregs and visualization of Tfr and HyHEL10 (Hy10) GC B cells in the dLNs by 2P microscopy. **b**, Flow cytometry analysis of the endogenous and transferred TdTomato^{+} Treg numbers in the blood of FoxP3^{DTR} mice throughout their treatments with DTx and immunization, performed as in (a). **c-e**, Analysis of dLNs from mice generated through the procedure described in (a) at 8 d.p.i. **c**, Representative flow cytometry analysis of Bcl6 expression in the CXCR5^{low}PD1^{low} and CXCR5^{high}PD1^{high} subsets of tdTomato^{+} Tregs (top panels), endogenous Tregs (middle panels) and endogenous Th cells (bottom panels). **d**, Confocal immunofluorescence analysis of dLN sections for the fraction of tdTomato^{+} cells that express Foxp3 (left bars) and fraction of Foxp3+ cells that express tdTomato^{+} (right bars) in GC-containing follicles.**e**, Representative 2P imaging analysis of Tfr cells localization with respect to GCs. A snapshot (left panel) from an intravital imaging experiment as analyzed in Imaris software. Cell trajectory analysis for Tfr cells (middle panel) and both Tfr cells and GC B cells (right panel). Scale bars 40 µm. Data are from 2 independent experiments.

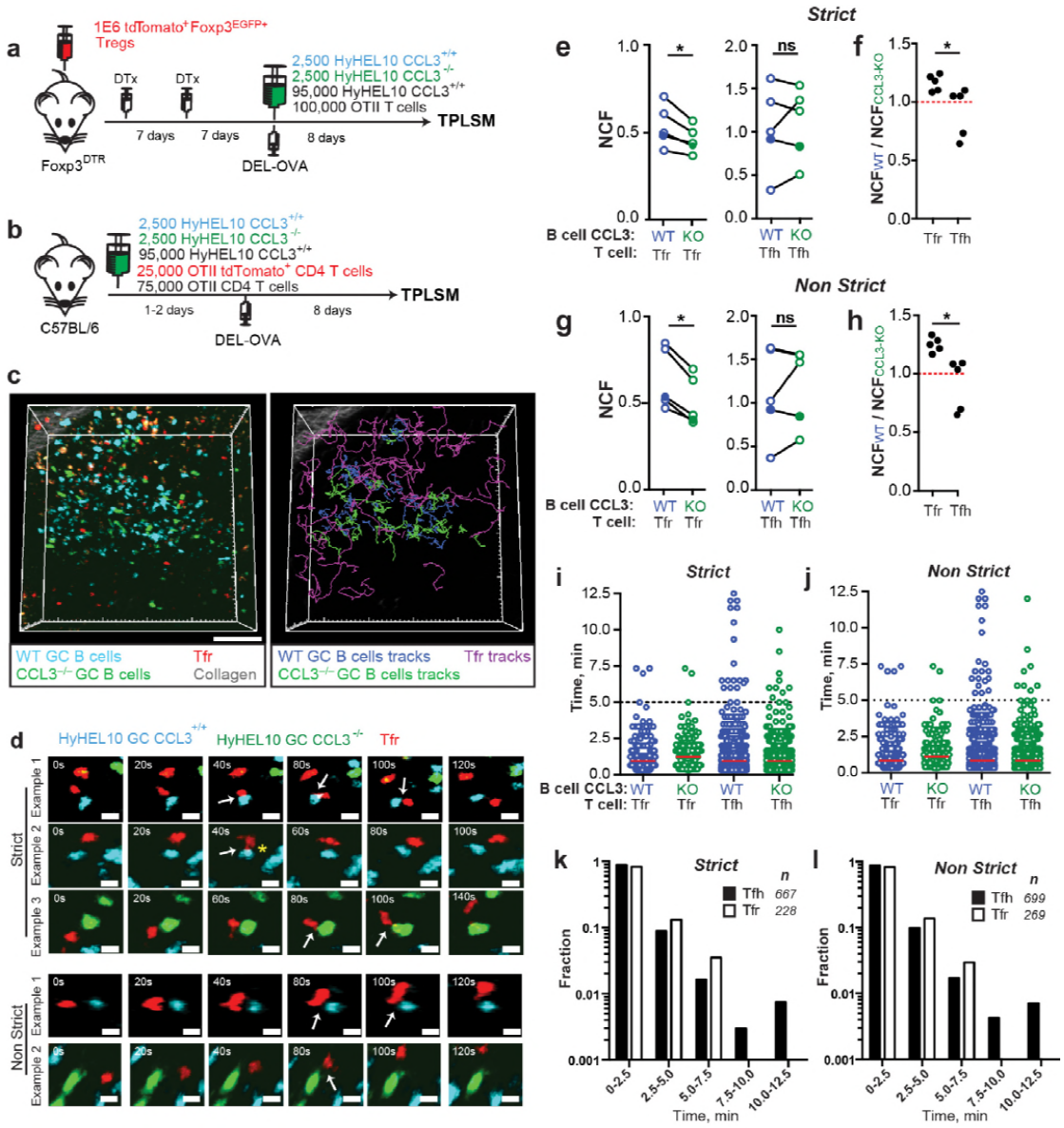

Figure 6. Tfr cells make less frequent contacts with CCL3-KO B cells in GCs. 2P imaging analysis of Tfr and Tfh cells contacts with CCL3$^{+/+}$ CFP and CCL3$^{-/-}$ GFP HyHEL10 GC B cells in the dLNs of mice at 8 d.p.i. **a, b**, Experimental diagrams for imaging GC B cell interactions with Tfr (a) and Tfh (b). **c**, A snapshot (**left panel**) and cell trajectory analysis (**right panel**) from an intravital imaging experiment performed as described in a**.** Scale bars - 50 μm. Auto-fluorescent cells are orange. **d,** Time-lapse images of Tfr cells interacting with CCL3$^{+/+}$ or CCL3$^{-/-}$ HyHEL10 B cells within GCs. Cell contacts were verified in 3D space, classified as Strict (definitive contacts) and Non Strict (all possible contacts) and indicated by white arrows. Yellow star illustrates pseudopod extension by a Tfr cell towards CFP GC B cell. Images are displayed as 20 μm z-stacks. Scale bars - 5 μm. **e-j**, Quantitative analysis of CCL3$^{+/+}$ (blue circles) and CCL3$^{-/-}$ (green circles) HyHEL10 GC B cell interactions with Tfr or Tfh cells. Closed symbols represent intravital and opened symbols - explanted dLNs imaging. The data was analyzed in a blinded fashion to avoid possible bias in cell contact definition. **e, g,** Normalized contact frequency (NCF) calculated for Strict (e) and Non Strict (g) as the number of Tfr or Tfh cells' interactions with CCL3$^{+/+}$ and CCL3$^{-/-}$ HyHEL10 B cells within defined volume of GCs normalized to the average number of HyHEL10 cells of each genotype. Linked symbols correspond to GC B

cells in the same movie. *, P<0.05, Wilcoxon matched-pairs test. **f, h,** Ratios of the Tfr or Tfh cell NCF with $CCL3^{+/+}$ over $CCL3^{-/-}$ HyHEL10 B cells from the same movie. *, P<0.05, Student's t-test. **i, j**, Contact duration between Tfr or Tfh and HyHEL10 GC B cells of each genotype undergoing Strict (i) or Non Strict (j) interactions. Red lines represent medians. Data from 5 independent experiments (5 mice) per T cell type. **k, l,** Time histograms for duration of strict (k) and non-strict (l) contacts between Tfr and Tfh cells with WT HyHEL10 GC B cells.

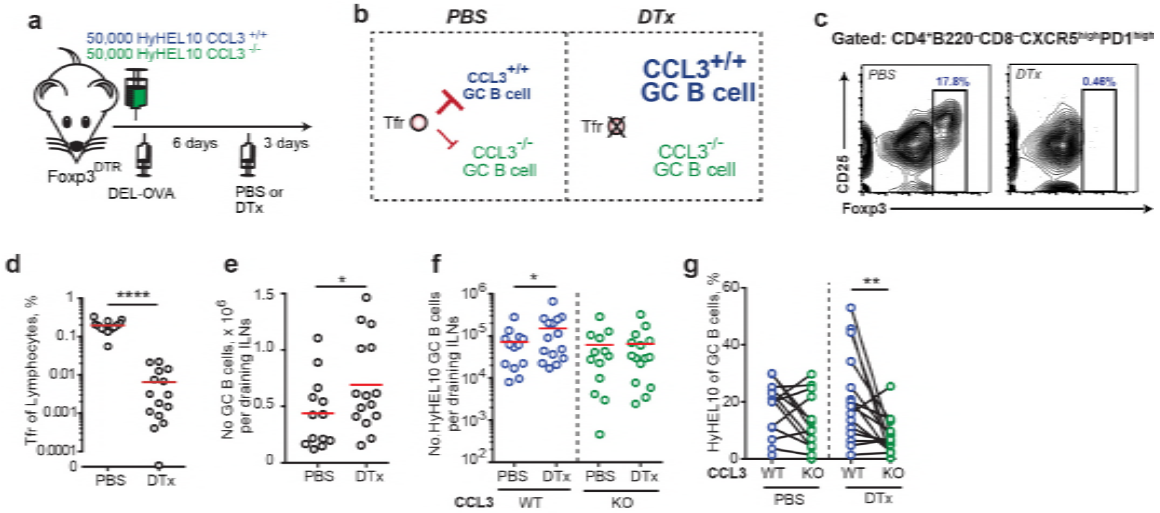

Figure 7. Tregs repress B cell participation in GCs at 9 d.p.i. in a CCL3-dependent way. a, Experimental outline. FoxP3^{DTR} recipient mice were transferred with HyHEL10 B cells, immunized with 50 µg DEL-OVA in Ribi s.c. and then treated either with PBS or 5 µg DTx in PBS i.p. 3 days before analysis. **b**, Suggested model of CCL3-dependent regulation of GC B cells by Tfr cells and prediction for CCL3$^{+/+}$ and CCL3$^{-/-}$ GC B cell participation in GCs upon ablation of Tfr cells at 9 d.p.i. **c-g**, Flow cytometry analysis of cell participation in immune response at 9 d.p.i. in DTx-treated and control mice. **c-e,** DTx-mediated depletion of Tfr cells at 9 d.p.i. Representative example of Tfr ablation (in c) and Tfr fraction of total lymphocytes (in d) and increase in GC response in DTx-treated mice (in e). **f, g,** CCL3$^{+/+}$ and CCL3$^{-/-}$ HyHEL10 GC B cells in PBS and DTx-treated mice shown as the total numbers of cells in dLNs (f) or as the % of total GC B cells. The data are from 5 independent experiments. Each dot represents a single mouse and red lines correspond to the mean values. Paired analyses are indicated using solid black line. *, $p<0.05$, **, $p<0.01$, ****, $P<0.0001$. Two-sided (in d, g) or one-sided (in e, f) Student's t-test.

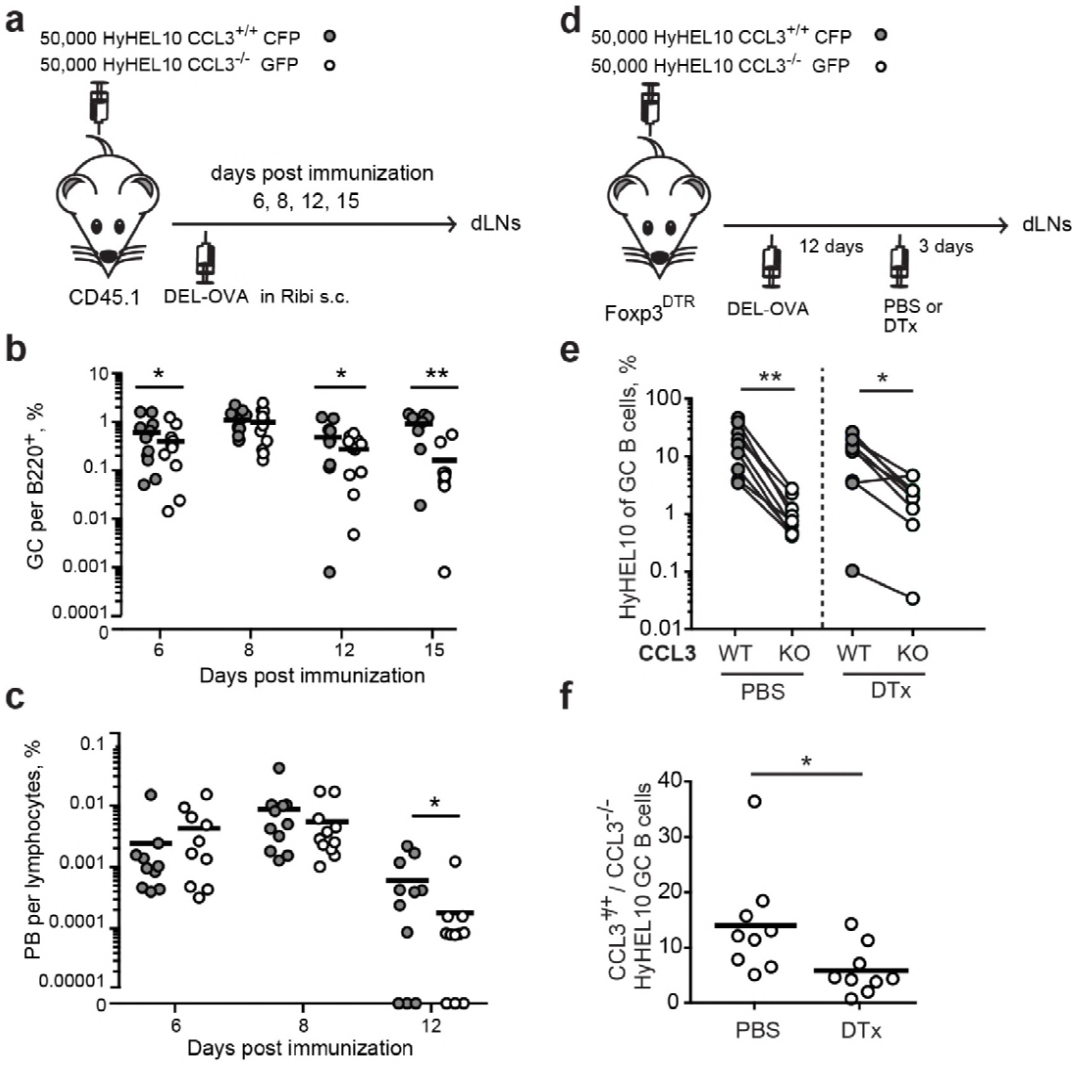

Figure 8. CCL3$^{+/+}$ foreign Ag-specific B cells outcompete CCL3$^{-/-}$ cells in GCs overtime. Flow cytometry analysis of HyHEL10 CCL3$^{+/+}$ B cells expressing cyan fluorescent protein (CFP, grey circles) and HyHEL10 CCL3$^{-/-}$ B cells expressing green fluorescent protein (GFP, white circles) recruitment and participation in B cells response in CD45.1 (a-c) or FoxP3^{DTR} (d-f) recipient mice following immunization. **a,** Experimental strategy. **b**, GC B cells as a % of total B cells. **c**, PB as a fraction of total lymphocytes. **d**, Experimental outline. FoxP3^{DTR} recipient mice were transferred with HyHEL10 B cells, immunized with 50 µg DEL-OVA in Ribi s.c. for 12 days and then treated either with PBS or 5 µg DTx in PBS i.p. 3 days before analysis. **e, f,** CCL3$^{+/+}$ and CCL3$^{-/-}$ HyHEL10 GC B cells in PBS and DTx-treated mice shown as the % of total GC B cells (e) or the ratio of CCL3$^{+/+}$ to CCL3$^{-/-}$ GC B cells. Data represents 3-5 independent experiments. Each symbol represents one mouse. Lines represent mean. Paired analyses are indicated using solid black line. *, P<0.05, **, P<0.01, Two-sided Student's *t*-test.

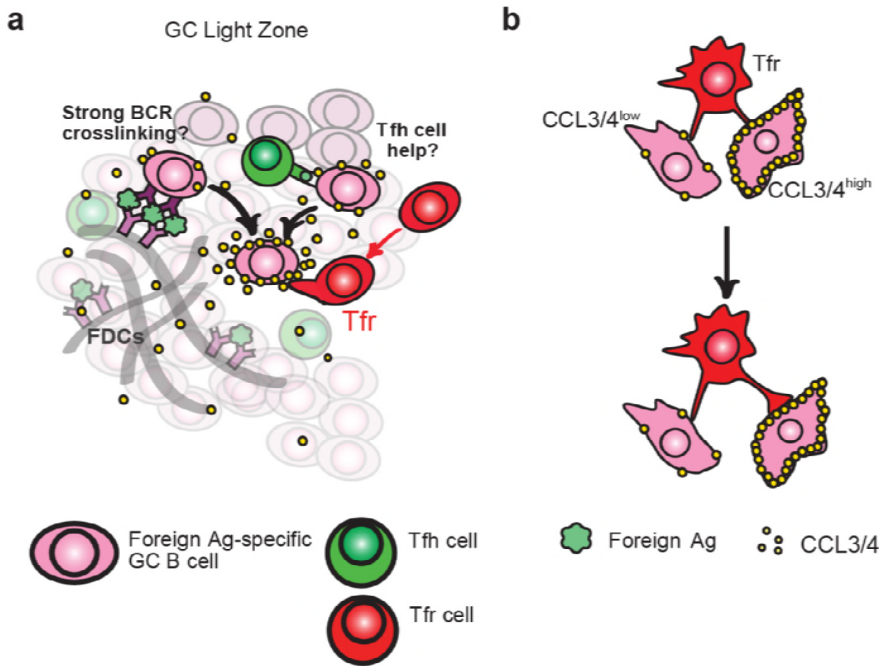

Figure 9: **A model of GC B cells' contacts with Tfr cells in CCL3-dependent fashion**. **a**, A model of local CCL3 gradients produced by selected GC B cells following strong BCR crosslinking (and/or T cell help). Local gradients could then enable enhanced chemotactic sampling of selected GC B cells by the rare Tfr cells traversing the GCs. **b,** A model of how secreted CCL3 immobilized on the surface of GC B cells may act to stabilize very transient probing interactions of Tfr cells with GC B cells that upon stabilization are visualized by 2P microscopy and result in more extensive GC B cell control.

1018 **SUPPLEMENTARY FIGURES**

1019

1020

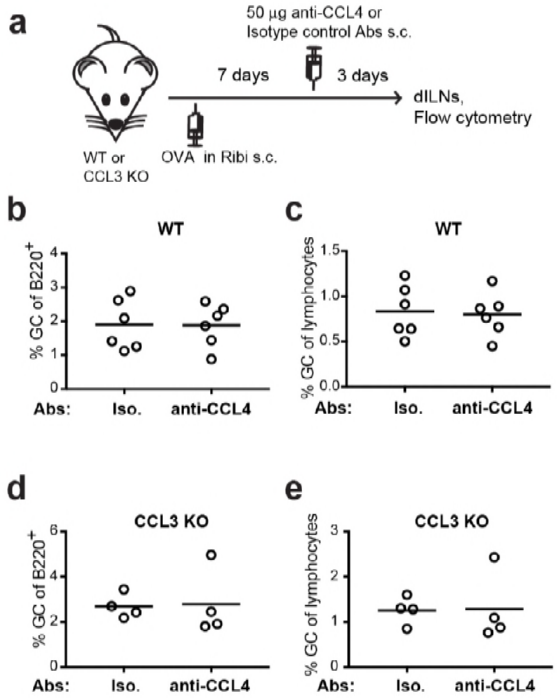

Supplementary Figure 2. CCL4 neutralization in GCs does not amplify GC response in WT or CCL3-KO mice. a, Experimental strategy. **b-e**, GC B cells ($B220^{pos}$ $CD4^{neg}$ $CD8^{neg}$ FAS^{high} $GL7^{high}$) in the dLNs of WT (b, c) and CCL3-KO (d, e) mice as a fraction of $B220^{+}$ cells (b, d) or lymphocytes (c, d) at 10 d.p.i. with OVA in Ribi.

1021

1022

1023

1024

1025

1026

1027

1028

1029

1030

1031

1032

1033

1034

1035

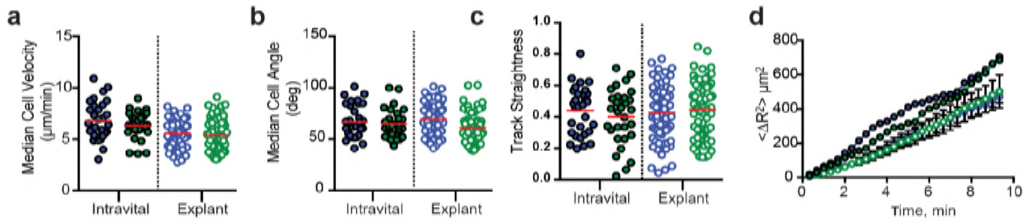

Supplementary Figure 6: HyHEL10 GC CCL3$^{+/+}$ CFP (blue circles) and CCL3$^{-/-}$ GFP (green circles) cell motility analysis. Red lines represent medians. Data are from 4 independent experiments.

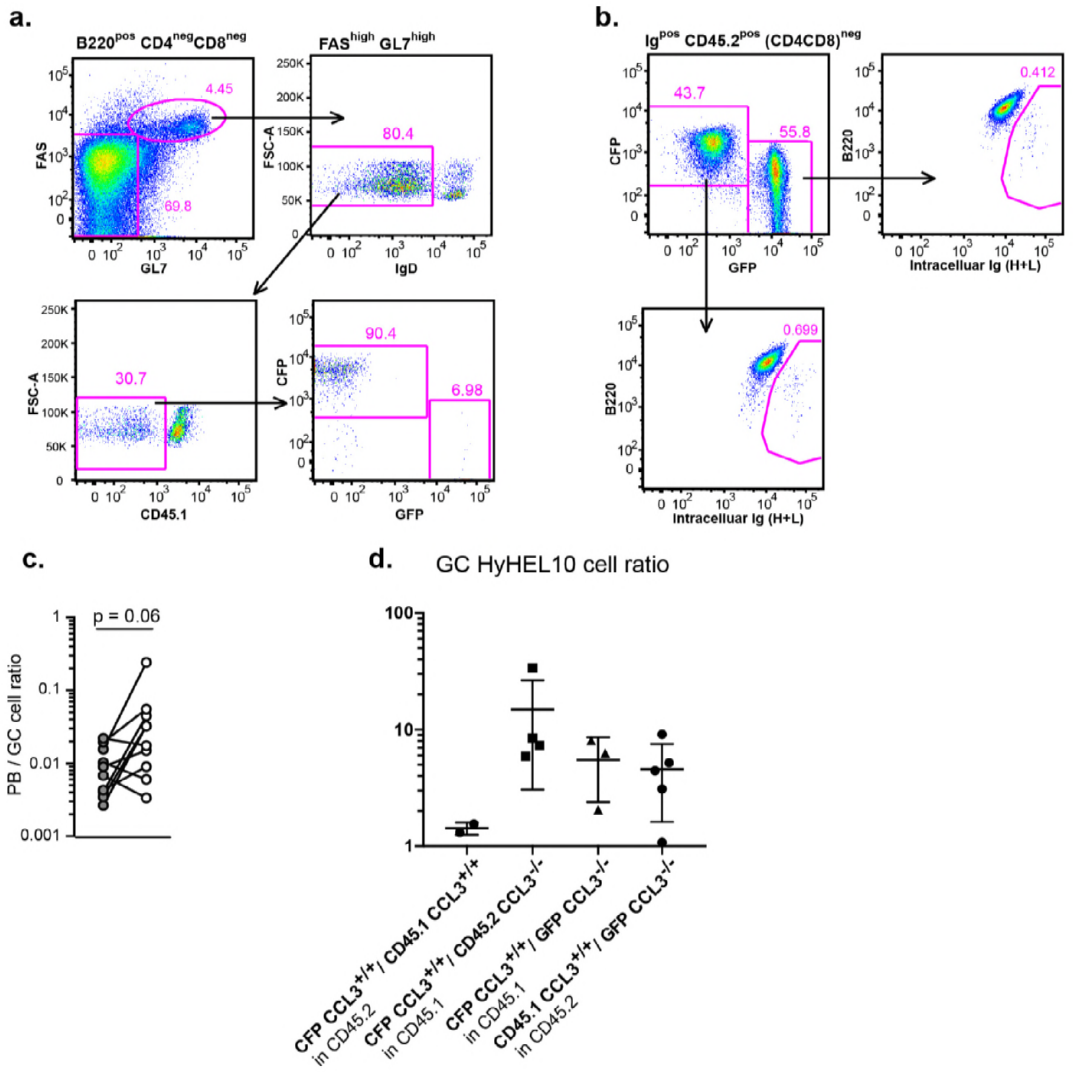

Supplementary Figure 8. Participation of CCL3$^{+/+}$ and CCL3$^{-/-}$ HyHEL10 B cells in the GC and PB response. a-c, CFP CCL3$^{+/+}$ and GFP CCL3$^{-/-}$ HyHEL10 B cells were cotransferred into CD45.1 recipient mice that were then immunized with DEL-OVA in Ribi as in Fig. 4a. **a,b,** The gating strategy for GC (in a) and PB (in b) CFP and GFP HyHEL10 cells. **c**, The ratio of PB to GC cells of CFP CCL3$^{+/+}$ (grey circles) and GFP CCL3$^{-/-}$ (white circles) HyHEL10 cells at 6 d.p.i. Data are from 4 independent experiments.Paired Student's t-test. **d**, Selection of CCL3$^{+/+}$ over CCL3$^{-/-}$ HyHEL10 cells in GCs at 12 d.p.i. In this experiment 5x10^5 HyHEL10 B cells were cotransferred into recipient mice, and more rapid selection of CCL3$^{+/+}$ HyHEL10 GC B cells was then observed. Data are from 2 independent experiments.

SUPPLEMENTARY MOVIE LEGENDS

Movie S1. 2-photon imaging of Tfr cells migration in respect to Tfh cells and GC B cells. Also see **Figure 5e**. A time-lapse sequence of a 110 µm z-stack of a GC in an explanted inguinal lymph node imaged at 8 days after immunization. HyHEL10 GC B cell; cyan. Tfr; red. Tfh; green. Colored lines indicate the trajectories of the indicated cell types, tracked by Imaris and manually verified. Mice were generated as described in the **Figure 5a**. Time is shown as hh:mm:ss and z-stacks were acquired at 20 second intervals.

Movie S2. Intravital imaging of Tfr cells in respect to the GCs containing both CCL3$^{+/+}$ and CCL3$^{-/-}$ HyHEL10 B cells. The data shown corresponds with the images in **Figure 6**. A time-lapse sequence of a GC within inguinal LN of a mouse prepared as described in **Figure 6a** and subjected to intravital imaging at 8 days post immunization. 180 µm z-stack. GC volume (gray surface) was defined based on the distribution of CFP HyHEL10 cells. Quantitative analysis in **Figure 6e-l** was performed for Tfr cells (red) interactions with HyHEL10 GC B cells (CCL3$^{+/+}$; cyan. CCL3$^{-/-}$; green.) within GC volumes defined in the same fashion. The tracks of individual Tfr cells outside the GC are labeled in purple while interior tracks are represented in yellow lines. Time is expressed as hh:mm:ss and z-stacks were acquired at 20 second intervals.

Movie S3. Examples of Tfr cells interactions with GC B cells identified as "strict" or "nonstrict" for quantitative analysis. A time-lapse sequence of a representative Tfr (red) entering the GC (dashed white line) and then undergoing contacts with HyHEL10 CCL3$^{+/+}$ (cyan) or CCL3$^{-/-}$ (green) HyHEL10 GC B cells within inguinal LN of a mouse prepared as described in **Figure 6a** and subjected to 2P imaging at 8 days post immunization. A 40 μM slice is in view. Inlets are zoomed in and 3D rotated to visualize the contact. Time is expressed as mm:ss and z-stacks were acquired at 25 second intervals

Movie S4. 2-photon imaging of Tfh cells interacting with GC B cells. A time-lapse sequence of a GC within an inguinal LN of a mouse prepared as described in **Figure 6b** and subjected to explant imaging at 8 days post immunization. 140 um z-stack**.** Quantitative analysis was performed for Tfh cells (red) interactions with HyHEL10 GC B cells (CCL3$^{+/+}$, cyan; CCL3$^{-/-}$, green) within the GC and can be found in **Figure 6e-l**. Examples of long duration (>5 minutes) contacts and short duration (<5 minutes) contacts are shown in 10 um z-projections. Time is shown as hh:mm:ss for both time of the movie and for duration of the indicated contacts. Z-stacks were acquired at 20 second intervals.